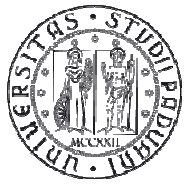

UNIVERSITY OF PADUA

DEPARTEMENT OF MANAGEMENT AND ENGINEERING

DOCTORAL SCHOOL OF INDUSTRIAL ENGINEERING
CURRICULUM IN MECHATRONICS AND INDUSTRIAL SYSTEMS
CYCLE XXIV

KINEMATIC INDEXES AND MODELS FOR PERFORMANCE OPTIMIZATION OF PARALLEL MANIPULATORS

Prof. PAOLO BARIANI, Chair of the School

Prof. ALBERTO TREVISANI, Curriculum Coordinator

Prof. GIOVANNI BOSCHETTI, Candidate's Supervisor

Ph.D. candidate: ROSSELLA ROSA

To my mother, Catia

SUMMARY

This Thesis proposes definitions of novel performance indexes for parallel manipulators. The first one, called Direction Selective Index (DSI), can provide uncoupled evaluations of robot translational capabilities along specific directions. Such an index, which might be considered an extension of the traditional manipulability index, overcomes the limitations of manipulability (but also of other popular indexes such as the minimum singular value and the condition number of the Jacobian matrix) which just provides global evaluations of the robot capabilities that are often of limited practical usefulness.

Afterwards, a new Task dependent Performance Index (TPI) has been defined based on the extended DSI formulation. TPI is an index aimed at providing evaluations of parallel robot performances in executing specific tasks. What is innovative in the TPI, is its accounting for robot kinematics and task geometrical features concurrently.

The experimental investigations carried out on a commercial parallel robot have proved the validity of the hints inferred through the proposed DSI formulation and the reliability of the TPI formulation predictions of the best relative positioning between the robot and the task to be executed.

The TPI has also been employed as a design tool in an optimization methodology for choosing the lengths of some selected robot links. Such a method as well as the proposed indexes can therefore be applied to any parallel robot architecture, as long as an inverse Jacobian matrix can be computed.

SOMMARIO

In questa Tesi vengono proposti nuovi indici di prestazione per manipolatori paralleli. Il primo, chiamato Direction Selective Index (DSI), consente di valutare separatamente le capacità di traslazione del robot lungo specifiche direzioni. Tale indice, che può essere considerato una estensione del tradizionale indice di manipolabilità, supera i limiti di quest'ultimo (oltre a quelli di altri indici conosciuti come il minimo valore singolare o il numero di condizionamento della matrice Jacobiana) che dà solo delle valutazioni globali delle capacità del robot che spesso non sono utili dal punto di vista pratico.

Successivamente, è stato definito un altro indice, il Task dependent Performance Index (TPI), basato sulla formulazione del DSI. Il TPI ha lo scopo di valutare le prestazioni del robot riguardanti l'esecuzione di specifiche operazioni. L'aspetto innovativo del TPI è rappresentato dal tener conto della cinematica del robot e delle caratteristiche geometriche dell'operazione.

Gli studi sperimentali condotti su un robot parallelo di uso commerciale hanno dimostrato la validità dei suggerimenti ottenuti attraverso il DSI e l'affidabilità delle previsioni del TPI nell'individuare la migliore posizione relativa tra robot e task da eseguire.

Inoltre il TPI è stato utilizzato come strumento di progettazione in un metodo di ottimizzazione per la scelta delle lunghezze di alcuni membri del robot. Una volta ricavata la matrice Jacobiana inversa del robot, gli indici proposti e il metodo di ottimizzazione possono essere applicati a qualsiasi manipolatore parallelo.

Acknowledgments

I would like to express gratitude to my supervisor Prof. Giovanni Boschetti and to Prof. Alberto Trevisani, Prof. Dario Richiedei and Prof. Roberto Caracciolo for their kind suggestions and support.

This research has been realized thanks to the support of FSU, Fondazione Studi Universitari Vicenza. I would like to express my sincere gratitude to the Foundation for having sponsored my Doctoral course throughout the tree years.

Ringraziamenti

Prima fra tutti vorrei ringraziare mia madre che ogni giorno rappresenta per me un esempio di forza e coraggio e mi ricorda quanto sia importante inseguire le proprie ambizioni e i propri sogni. Poi tutta la mia famiglia, mio padre, i miei fratelli e la mia nipotina Anna, che con calore e affetto mi sostengono nelle scelte che la vita impone di fare. La solidità che ci unisce dà forza al nostro rapporto.

In questi tre anni ho potuto conoscere persone che mi hanno fatto comprendere quanto sia importante impegnarsi in tutto ciò che si fa, tra questi Alberto, Dario, Giovanni e il Prof. Caracciolo. Mettono grande passione nel proprio lavoro e a loro va tutta la mia stima.

Vorrei poi ringraziare tutti i colleghi che hanno condiviso con me questo periodo, in particolare Gabriele, collega e amico, e Manuel. Ringrazio tutti gli amici e tutti coloro che credono nelle mie capacità e desidero ricordare Federico, grande amico da sempre, ed Elisa, con la quale sono cresciuta e a cui devo molto. Anche se la vita ci ha portato ora a percorrere strade diverse, sento dal cuore di dover dire grazie a Enrico, per diversi anni mi è stato vicino e ho avuto il piacere di crescere insieme a lui.

…*"Ciascuno di noi è, in verità, un'immagine del Grande Gabbiano, un'infinita idea di libertà, senza limiti"*.

Contents

INTRODUCTION

The scope of this Thesis is to provide novel performance indexes specifically developed for parallel manipulators and innovative methods for computing the geometrical synthesis of robot or optimizing the location of tasks within the manipulator workspace.

Performance indexes usually provide global evaluations of robot performances mixing their translational and/or rotational capabilities. This Thesis proposes a definition of a novel performance index, called Direction Selective Index (DSI) which can provide uncoupled evaluations of robot translational capabilities along specific directions. Such indexes, which might be considered an extension of the traditional manipulability index, overcome the limitations of manipulability (but also of other popular indexes such as the minimum singular value and the condition number of the Jacobian matrix) which just provides global evaluations of the robot capabilities that are often of limited practical usefulness.

The DSI formulation is first presented within a general framework, highlighting its relationship with traditional manipulability definitions, and then applied to a family of parallel manipulators (4-RUU) of industrial interest. The investigation is both numerical and experimental, and allows highlighting the two chief advantages of the proposed DSIs over more conventional manipulability indexes: not only are DSIs more accurate in predicting the workspace regions where manipulators can best perform translational movements along specific directions, but also they allow foreseeing satisfactorily the dynamic performance variations

within the workspace, though being purely kinematic indexes. The experiments have been carried out on an instrumented 4-RUU commercial robot.

The experimental investigation has been done mainly because the numerical results highlight major differences in the best performance regions identified by the DSIs and the manipulability indexes. The experiments have been carried out by instrumenting the robot with MEMS accelerometers and by making the robot perform extensive tests consisting in constant-length vertical and horizontal movements of the moving platform within the whole workspace: the expected and the real performances of the robot have then been compared. The results from the experimental investigation prove the validity of the hints inferred through the proposed DSI formulation and hence its practical usefulness. In particular, as theoretically expected, DSIs turn up to be far more descriptive than manipulability.

Performance indexes can provide essential contributions to such an evaluation, in particular if they can account for the specific task with respect to which optimization is carried out.

This Thesis introduces a performance index for parallel manipulators called Task dependent Performance Index (TPI), which explicitly accounts for both robot kinematics and task geometrical features. It is proved that TPI can provide accurate evaluation of robot performances in executing generic tasks though being a purely kinematic index. Hence, optimal robot/task relative positioning can be straightforwardly achieved by maximizing the proposed TPI.

The TPI formulation is based on the one of Direction Selective perfomance Index (DSI). In particular, the TPI definition explicitly accounts for the length and

direction of the sequence of translations to be accomplished by a robot to carry out a task.

As a proof of concept, the TPI formulation has been employed in a maximization algorithm in order to optimize the location of some pick-and-place tasks within the workspace of an industrial 4-RUU parallel robot. The experimental results collected provide adequate evidence of the effectiveness of the proposed index and of its usefulness in optimal robot positioning.

Considering that performances of parallel robots are very sensitive to the mechanism dimensions, the geometrical synthesis of the mechanisms cannot be dissociated from the analysis of performance indices or criterions for characterizing the behavior of manipulators. In literature there has not been a unified method for the robot design and it can be of primary importance to study some useful methods which allow to understand the relationships between the criteria and link lengths of the manipulators.

The experimental validation of DSI and TPI has led to develop a geometric optimization of parallel robot link lengths based on TPI maximization.

The Thesis is organized as follows. In the first Chapter a literature review on the performance indexes is proposed. The adaptation for parallel manipulators of some indexes firstly employed for serial ones is considered. In the second Chapter the DSI formulations suitable for displacements along the axes of the robot world reference frame first and then along generic directions are proposed. Moreover the DSI definition is applied to the family of 4-RUU parallel manipulators. The results of a numerical investigation aimed at assessing and comparing the shapes of the DSIs and of manipulability indexes within the workspace of the Quattro robot are

shown. Planar and spatial graphical representations of the shapes of the indexes are provided. The experimental campaign and its results are then presented and discussed. Then, in Chapter 3, the proposed task-dependent index TPI is explicitly introduced. Its definition is applied to the family of 4-RUU parallel manipulators and a numerical investigation is carried out to stress the differences between DSI and TPI performance predictions. The optimal location problem is discussed in Chapter 4. The results of the experimental tests carried out to prove the effectiveness of TPI and of the maximization algorithm exploiting TPI formulation are shown. A through comparison is performed between numerical expectations and experimental measurements. In particular, with reference to the TPI, the time taken to carry out several pick-and-place tasks is compared with the TPI values. The comparison proves a satisfactory adherence between the TPI performance variation predictions and the robot actual performances. It is shown that, an optimal relative positioning between the robot and the task can be straightforwardly achieved by maximizing the TPI. Chapter 5 is focus on the optimization problem of choosing the lengths of some selected robot links maximizing the TPI. The optimization methodology proposed is illustrated with examples involving the four-leg delta-like Adept Quattro parallel manipulator.

Finally, concluding remarks are provided in the Conclusions.

1 PERFORMANCE EVALUATION OF PARALLEL ROBOTS

1.1. Literature review

1.1.1. Performance Indexes

Performance evaluation is one of most important issues in the analysis and design of manipulators. Indeed performance indexes may provide useful hints in the design and optimization of robots. Such indexes can be defined for all kinds of robotic mechanical systems and we focus here on those referred to robots manipulability and dexterity. Dexterity represents the ability of a mechanism to move and apply forces in arbitrary directions as easily as possible.

In particular, a distinction can be made between local and global dexterity. The local one characterize a mechanism dexterity at a given posture, while global dexterity measures the overall dexterity of a mechanism.

In 1982, Salisbury and Craig firstly proposed a measure of local dexterity when working on the design of articulated hands [SALISBURY 1982A]. Such a measure of the workspace quality is the condition number of the transpose of the Jacobian matrix $\boldsymbol{J}$:

$$k=\mathrm{cond}(\boldsymbol{J}^{\mathrm{T}}) \tag{1.1}$$

Some years later, Yoshikawa introduced the concept of manipulability, bases on Jacobian matrix:

$$\mu = \sqrt{det(\boldsymbol{J} \cdot \boldsymbol{J}^{\mathrm{T}})} \tag{1.2}$$

in order to find the best postures for manipulators [YOSHIKAWA 1985].

The minimum singular value is another performance index which can be used to put an upper bound on required joint velocities [KLEIN 1987]. It is defined as:

$$\sigma_{\min}(\boldsymbol{J} \cdot \boldsymbol{J}^{\mathrm{T}}) \tag{1.3}$$

It indicates situations where excessive joint velocities would be required, which is a characteristic of nearness to singularities.

Subsequently, the reciprocal of the condition number discussed in [SALISBURY 1982B], i.e. $1/k$, has been defined as the local conditioning index (LCI) to evaluate the control accuracy, dexterity and isotropy of the mechanism [ANGELES 1988]. In order to evaluate the dexterity of a robot over a given workspace, the following adaptation is used by Gosselin and Angeles in [GOSSELIN 1991]. Such an index is basically an integral mean of the condition number:

$$\mathrm{GCI} = \frac{\int_W (1/k) dW}{\int_W dW} \tag{1.4}$$

1.1.2. Performance Indexes adaptation for Parallel Robots

In [MERLET 2006] the definitions of manipulability, condition number, and dexterity index have been revisited in order to be applied to parallel robots. Novel formulations have been proposed, which are different from the ones introduced in [SALISBURY 1982], [YOSHIKAWA 1985], [KLEIN 1987], [ANGELES 1988], [GOSSELIN 1991].

Performance indexes based on Jacobian matrix may be affected by the presence of inhomogeneities in the velocity ratios that may lead to ineffective results. Such a problem was found in [ANGELES 1992] in the analysis of the Jacobian matrix of serial manipulators. It was solved by defining a characteristic length of the manipulator and by proposing a weighting positive matrix that allows obtaining a homogenous Jacobian. Unfortunately such a solution cannot be easily extended to parallel manipulators. The first formulation of a dimensionally homogeneous Jacobian matrix overcoming this problem for planar parallel manipulators was introduced in [GOSSELIN 1992]. Such a Jacobian relates the actuator velocities to the ones of the Cartesian coordinates of two points of the mobile platform.

Following such a reasoning, in [KIM 2003] a new dimensionally homogeneous Jacobian matrix was formulated by relating the velocities of three points (coplanar with the mobile platform joints) to the actuator ones. The same approach has been proposed in [KIM 2004] for force transmission analysis and then it has been reformulated in [POND 2006] for the dexterity analysis of parallel manipulators.

A simple performance index based on Jacobian matrix has been also presented in [MAYORGA 2006]. The proposed index is derived by developing an upper

bound on the norm of the rate of change of the Jacobian matrix. Such an upper bound has a significant role in a sufficiency condition for Jacobian rank preservation. It is proved that the index proposed in [POND 2006] provides information coherent with manipulability [YOSHIKAWA 1985] and the condition number [SALISBURY 1982], while being easier to compute.

In [LI 2006A] the dexterity index has been exploited together with a space utility ratio in order to compose a mixed performance index for optimizing translational parallel manipulators. The introduction of the space utility ratio index ensures avoiding disproportion between the reachable workspace volume and the structure of the robot by using the ratio between the total workspace volume and the physical size of the manipulator.

A performance investigation on translational parallel manipulators has been presented in [XU 2008]. The performance index is given by the minimum and the maximum eigenvalues of the stiffness matrix obtained from the Jacobian as proposed in [GOSSELLIN 1990]. The effectiveness of this index has been proved by applying it to an innovative parallel manipulator whose kinematics is analyzed in [LI 2006B].

Successively, in [MANSOURI 2009] and [MANSOURI 2011] a kinetostatic performance index, called Power Manipulability has been introduced. Power Manipulability is related to the power within the mechanism, and is fully homogeneous, whether the manipulator contains active joints of different type, or the task space combines both translation and rotation motion.

A different approach for the computation of manipulator dexterity has been proposed in some recent studies ([WANG 2009] and [WANG 2010]), where a

generalized transmission index that can evaluate the motion/force transmissibility of fully parallel manipulators has been defined through virtual coefficients and not through Jacobian matrix. Contrary to the other indexes, such a transmission index is frame-free (i.e. its value does not depend on the reference frame in which it is computed).

Moreover, it can be used to identify a good transmission workspace, where not only is the parallel manipulator effective in terms of motion/force transmission, but also far from its singularities.

1.1.3. Manipulability Indexes

All the aforementioned indexes provide global evaluations of robot performances mixing the translational capabilities of robots or the rotational ones. However in [MERLET 2006] the concept of manipulability has been extended to evaluate the translational and rotational capabilities of parallel manipulators. In such a case the Jacobian matrix has been split in two submatrices, $\boldsymbol{J}_t$ and $\boldsymbol{J}_r$, evaluated separately.

The congruence equation of the position analysis of a parallel manipulator can be generally defined as $\boldsymbol{F}(\boldsymbol{q}, \boldsymbol{x}) = \boldsymbol{0}$, where $\boldsymbol{q}$ denotes the joint variable vector, $\boldsymbol{x}$ the generalized coordinates of the end effector, $\boldsymbol{F}$ is an n-dimensional implicit function of $\boldsymbol{q}$ and $\boldsymbol{x}$, and $\boldsymbol{0}$ is the n-dimensional zero vector. By differentiating the congruence equation with respect to time, the velocity relation $\boldsymbol{J}_x \cdot \dot{\boldsymbol{x}} - \boldsymbol{J}_q \cdot \dot{\boldsymbol{q}} = \boldsymbol{0}$ is achieved, where $\boldsymbol{J}_x = \partial f_i / \partial x_j$ and $\boldsymbol{J}_q = -\partial f_i / \partial q_k$.

The two matrices $\boldsymbol{J}_x$ and $\boldsymbol{J}_q$ are the $n \times n$ Jacobian matrices of respectively the end-effector coordinates and the joint variables. Such matrices obviously depend on the configuration of the manipulator. From these equations there immediately follow the expressions of $\boldsymbol{J} := \boldsymbol{J}_x^{-1} \cdot \boldsymbol{J}_q$ and $\boldsymbol{J}^{-1} := \boldsymbol{J}_q^{-1} \cdot \boldsymbol{J}_x$ and also the solutions of the forward ($\dot{\boldsymbol{x}} = \boldsymbol{J} \cdot \dot{\boldsymbol{q}}$) and of the inverse ($\dot{\boldsymbol{q}} = \boldsymbol{J}^{-1} \cdot \dot{\boldsymbol{x}}$) velocity kinematic problems.

In parallel robotics forward position kinematics is usually harder to solve than inverse kinematics. Sometimes the analytical solution of the forward problem is not even available. Hence the analytical expression of the inverse Jacobian matrix $\boldsymbol{J}^{-1}$ is usually easier to achieve than $\boldsymbol{J}$.

One of the most popular performance indexes is the manipulability index whose formulation is reported in equation (1.2). Such an index was conceived for serial robots, hence it is based on the Jacobian matrix of the forward kinematic problem. However, as previously discussed, in parallel manipulators the inverse Jacobian matrix is usually available, which suggests introducing some small changes to the index definition. By recalling that if λ_i are the eigenvalues of a generic square matrix, the eigenvalues of its inverse are $1/\lambda_i$, and that the determinant of a matrix is equal to the dot product of its eigenvalues, a definition of the manipulability more suitable to parallel manipulators can be inferred:

$$\mu = \frac{1}{\sqrt{det(\boldsymbol{J}^{-\mathrm{T}} \cdot \boldsymbol{J}^{-1})}} \tag{1.5}$$

By making use of such a definition, the values of μ become comparable with those computed through Yoshikawa's formulation, and become identical to such values in case of square Jacobian matrices. Moreover, the values taken by μ are coherent with the singularity analysis for parallel robots defined in [21].

Other measure criteria of manipulability can be used in the performance analysis of parallel manipulators [MERLET 2006]: manipulability can indeed be also defined by means of

- the Euclidean norm (or Frobenius norm) $\|\boldsymbol{J}\cdot\boldsymbol{J}^{\mathrm{T}}\|_{\boldsymbol{F}}=\sqrt{\sum_{i,j=1}^{n}\left|a_{ij}\right|^{2}}$
- the infinity norm $\|\boldsymbol{J}\cdot\boldsymbol{J}^{\mathrm{T}}\|_{\infty}=max_{1\le i\le m}\sum_{j=1}^{n}\left|a_{ij}\right|$

where a_{ij} are the elements of the matrix $\boldsymbol{J}\cdot\boldsymbol{J}^{\mathrm{T}}$. By following a reasoning similar to the one leading to Eq.(1.2) from Eq.(1.5), the following further definitions of manipulability can be provided for parallel manipulators:

$$\mu^{F}=\frac{\mathbf{1}}{\|\boldsymbol{J}^{-\mathrm{T}}\cdot\boldsymbol{J}^{-1}\|_{F}} \tag{1.6}$$

$$\mu^{\infty}=\frac{\mathbf{1}}{\|\boldsymbol{J}^{-\mathrm{T}}\cdot\boldsymbol{J}^{-1}\|_{\infty}} \tag{1.7}$$

In order to try discriminating the performances related to linear and rotational displacements of the end-effector of a robot, the Jacobian matrix may be split into two parts, $\boldsymbol{J}_t$ and $\boldsymbol{J}_r$ ($\boldsymbol{J}=[\boldsymbol{J}_t\,|\,\boldsymbol{J}_r]^{\mathrm{T}}$), which can be evaluated separately [MERLET 2006]. The submatrix $\boldsymbol{J}_t$ contains the ratios between the end-effector translations

and the joint displacements; the submatrix $\boldsymbol{J}_r$ the ratios between the end-effector rotations and the joint displacements. Hence, different performance indexes can be computed making use of $\boldsymbol{J}_t$ and $\boldsymbol{J}_r$. Of course, such indexes still provide a global evaluation of the performances mixing either the translational capabilities of robot in the three directions or the rotational ones.

When parallel robots are considered, $\boldsymbol{J}_t$ and $\boldsymbol{J}_r$ are more easily computed through inverse kinematics: consider

- the matrix $\boldsymbol{J}_{xt}$, submatrix of $\boldsymbol{J}_x$ comprising the partial derivates with respect to the translational coordinates of the end-effector,
- the matrix $\boldsymbol{J}_{xr}$, submatrix of $\boldsymbol{J}_x$ comprising the partial derivates with respect to the rotational coordinates of the end-effector.

In the following Eq.(1.8) the matrices $\boldsymbol{J}_t^{-1}$ and $\boldsymbol{J}_r^{-1}$ are then the inverse matrices for the translational and the rotational inverse velocity analyses:

$$\boldsymbol{J}_t^{-1} = \boldsymbol{J}_q^{-1} \cdot \boldsymbol{J}_{xt} \qquad \boldsymbol{J}_r^{-1} = \boldsymbol{J}_q^{-1} \cdot \boldsymbol{J}_{xr} \tag{1.8}$$

The analyses based on the Jacobian submatrix $\boldsymbol{J}_t^{-1}$ and the values of the performance indexes that may be computed from such a matrix, are usually affected by the units adopted to measure the end-effector velocities and the joint ones. Some “normalization” criteria hence need to be adopted to make the results of the analyses comparable regardless of the features of the manipulator active joints (see references [KIM 2003] and [MA 1991]). As the matter of fact the coefficients of $\boldsymbol{J}_t^{-1}$ are the ratios between the linear velocities of the end effector,

and the velocities of the active joints, which might be either translational or rotational. In case of fully translational joints, the analysis of the matrix $\boldsymbol{J}_t^{-1}$ can be directly performed and leads to dimensionless indexes. Alternatively, if active joints are rotational, in order to keep the performance indexes dimensionless it may be appropriate to modify the elements of matrix $\boldsymbol{J}_t^{-1}$ so as to relate the end-effector translational velocities to the tangent velocities of the drive cranks, rather than to their angular velocities. A new dimensionless matrix $\boldsymbol{J}_{Dt}^{-1}$ can therefore be adopted when the active joints are rotational: $\boldsymbol{J}_{Dt}^{-1}$ is obtained by pre-multiplying $\boldsymbol{J}_t^{-1}$ by a diagonal matrix $\boldsymbol{D}$ made up of the lengths of the drive cranks:

$$\boldsymbol{J}_{Dt}^{-1} = \boldsymbol{D} \cdot \boldsymbol{J}_t^{-1} \qquad \boldsymbol{J}_{Dt} = \boldsymbol{J}_t \cdot \boldsymbol{D}^{-1} \tag{1.9}$$

By replacing $\boldsymbol{J}^{-1}$ (and its transpose matrix) in Eqs. (2), (3), and (4), with $\boldsymbol{J}_t^{-1}$ or $\boldsymbol{J}_{Dt}^{-1}$ (and its transpose matrix), according to the features of the active joints, it is possible to get the manipulability indexes referring to end-effector translational degrees of freedom. In particular, in case of fully rotational active joints, it holds:

$$\mu_t = \frac{1}{\sqrt{det\left(\boldsymbol{J}_{Dt}{}^{-\mathrm{T}} \cdot \boldsymbol{J}_{Dt}{}^{-1}\right)}} \tag{1.10}$$

$$\mu_t^F = \frac{\mathbf{1}}{\left\|\boldsymbol{J}_{Dt}^{-\mathrm{T}} \cdot \boldsymbol{J}_{Dt}^{-1}\right\|_F} \tag{1.11}$$

$$\mu_t^{\infty} = \frac{\mathbf{1}}{\left\| \boldsymbol{J}_{Dt}^{-\mathrm{T}} \cdot \boldsymbol{J}_{Dt}^{-1} \right\|_{\infty}} \tag{1.12}$$

Hence, the obtained manipulability indexes permit to distinguish the end-effector translational degrees of freedom from the rotational ones.

2 DEVELOPMENT OF DIRECTION SELECTIVE INDEX FOR PARALLEL ROBOT TRANSLATIONAL PERFORMANCE EVALUATION

2.1. Direction Selective Index (DSI)

The direction selective index (DSI) allows evaluating independently the translational capabilities, and hence the performances, of a parallel manipulator along the axes of its world reference frame.

The idea behind DSIs relies on further splitting matrices $\boldsymbol{J}_t^{-1}$ or $\boldsymbol{J}_{Dt}^{-1}$ into three column vectors in order to analyze robot performances along specific directions. As an example the following holds in case of fully rotational active joints:

$$\boldsymbol{J}_{Dt}^{-1} = [\boldsymbol{J}_X^{-1} \mid \boldsymbol{J}_Y^{-1} \mid \boldsymbol{J}_Z^{-1}] \tag{2.1}$$

The meaning of these column vectors is apparent: for example $\boldsymbol{J}_X^{-1}$ contain the velocity ratios between translations along the *X* axis of the world reference frame and rotations of the joints. In other words, it describes the effect on the joints of displacements along the *X* axis. Keeping this in mind, the DSI can then be straightforwardly defined by replacing $\boldsymbol{J}^{-1}$ (and its transpose matrix) with $\boldsymbol{J}_\rho^{-1}$ (and its transpose vector) in Eq.(1.5):

$$\mu_\rho = \frac{1}{\sqrt{det\left(\boldsymbol{J}_\rho^{-T} \cdot \boldsymbol{J}_\rho^{-1}\right)}} \tag{2.2}$$

Where ρ can be any direction X, Y or Z of the world reference frame.

The DSIs μ_X, μ_Y and μ_Z are here proposed to evaluate independently the translational capabilities of a manipulator along the axes of its world reference frame.

The performances along any other relevant direction can be straightforwardly evaluated by suitably rotating the world reference frame so that one axis coincides with the selected direction.

Let us consider a generic direction of motion *R* (see Fig. 2.1)

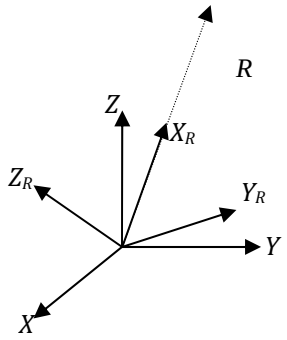

Fig. 2.1 Schematic representation of the world reference frame and of a rotated reference frame with the X_R axis parallel to the generic direction *R*.

Let us introduce a reference frame (X_R, Y_R, Z_R) with the X_R axis parallel to the direction of motion *R*, and the other axis arbitrarily oriented.

Let us denote with $\boldsymbol{R}$ the rotational matrix that describes the orientation of the reference frame (X_R, Y_R, Z_R) with respect to the world reference frame (X, Y, Z).

Starting from the solutions of the forward ($\dot{\boldsymbol{x}} = \boldsymbol{J} \cdot \dot{\boldsymbol{q}}$) and of the inverse ($\dot{\boldsymbol{q}} = \boldsymbol{J}^{-1} \cdot \dot{\boldsymbol{x}}$) velocity kinematic problems, we can consider that any translational velocity $\dot{\boldsymbol{x}}_R$ of the end-effector along the X_R axis can be expressed in the world reference frame by means of the following relation:

$$\dot{\boldsymbol{x}}_t = \boldsymbol{R} \cdot \dot{\boldsymbol{x}}_R \tag{2.3}$$

Moreover for linear displacement we can write:

$$\dot{\boldsymbol{q}} = \boldsymbol{J}_t^{-1} \cdot \dot{\boldsymbol{x}}_t \tag{2.4}$$

where vector $\dot{\boldsymbol{x}}_t$ is the translational part of $\dot{\boldsymbol{x}}$ ($\dot{\boldsymbol{x}} \coloneqq \{\dot{\boldsymbol{x}}_t^T | \dot{\boldsymbol{x}}_r^T\}^T$).

Afterwards, by defining $\dot{\boldsymbol{q}}_D = \boldsymbol{D} \cdot \dot{\boldsymbol{q}}$ the following velocity equation can be written:

$$\dot{\boldsymbol{q}}_D = \boldsymbol{J}_{Dt}^{-1} \cdot \dot{\boldsymbol{x}}_t \tag{2.5}$$

The dimensionless matrix $\boldsymbol{J}_{Dt}^{-1}$ can be adopted when active joints are rotational. Equation (2.5) can hence be rewritten in the form:

$$\dot{\boldsymbol{q}}_D = \boldsymbol{J}_{Dt}^{-1} \cdot \boldsymbol{R} \cdot \dot{\boldsymbol{x}}_R \tag{2.6}$$

where the column vectors of the matrix $\boldsymbol{J}_{Dt}^{-1} \cdot \boldsymbol{R}$ can be denoted as follows:

$$\boldsymbol{J}_{Dt}^{-1} \cdot \boldsymbol{R} := [\boldsymbol{J}_{XR}^{-1} \mid \boldsymbol{J}_{YR}^{-1} \mid \boldsymbol{J}_{ZR}^{-1}] \tag{2.7}$$

$\boldsymbol{J}_{XR}^{-1}$ contains the velocity ratios between an end-effector translation along the generic direction *R* and the congruent joint rotations.

There immediately follows that the DSI formulation μ_R accounting for translations along a generic direction *R* is:

$$\mu_R = \frac{1}{\sqrt{det(\boldsymbol{J}_{XR}^{-\mathrm{T}} \cdot \boldsymbol{J}_{XR}^{-1})}} \tag{2.8}$$

2.2. DSI formulation for 4-RUU Parallel Manipulators

2.2.1. The translational Jacobian matrix of an Industrial 4-RUU Manipulator

In order to assess the capability of the proposed indexes to foresee manipulator performance variations along selected directions, the definitions provided for μ_ρ, and μ_R have been applied to a generic 4-RUU parallel manipulator.

4-RUU manipulators are four-leg and four-degree-of-freedom parallel manipulators conceived for performing high-speed and high-acceleration pick-and-place operations. The kinematic and dynamic models for this family of parallel robots is reported in [COMPANY 2009]. Due to their architecture these robots can produce Schöenflies motions (i.e. translations along the *X*, *Y* and *Z* direction and a rotation about the *Z* axis), which are required in most pick-and-place operations,

including packaging, picking, packing and palletizing tasks. Figure 2.2 shows a picture of the robot and schematically depicts its architecture, its workspace, the location of its world reference frame and the workspace chief geometrical parameters. In Fig.2.2(b) it has been highlighted that the location of the center of the mechanical interface (and consequently the tool center point (TCP) in case no tool is defined or connected to the interface) is offset from the center of the moving platform by a distance equal to *p* in the positive *X* direction. As a result of the platform design, the relative position between the center of the platform and that of the mechanical interface does not change after translations or rotations. All the numerical and experimental analyses carried out in this work are referred to the tool center point, being such a point of chief interests for the robot user. The robot moving platform takes the shape of a rhombus whose side has length *2d*. The platform is connected to the fixed base by four identical RUU serial chain legs, i.e. legs with one revolute (R) and two universal (U) joints (see Fig.2.2).

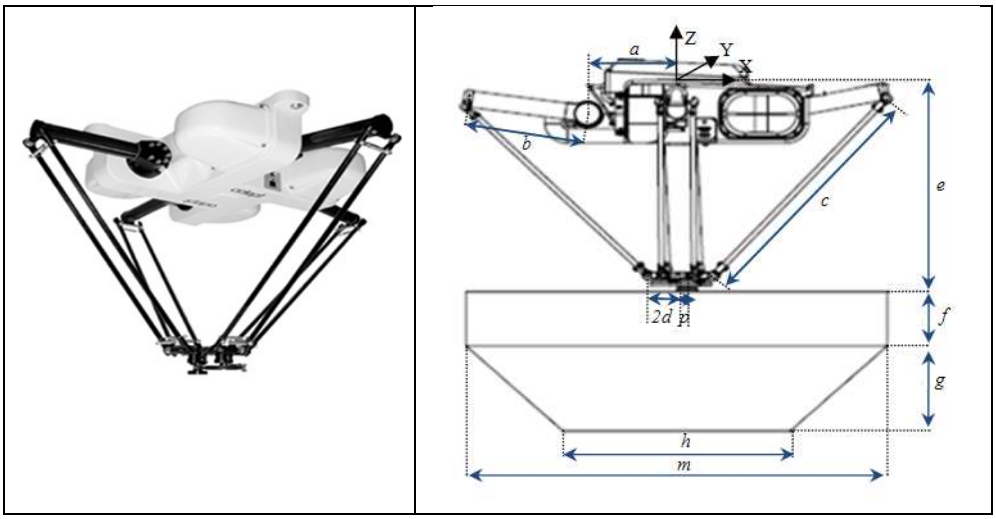

Fig. 1.2 Picture and schematic representation of the Adept Quattro^{TM} and of its workspace.

The values of the workspace and geometrical parameters are collected in Table 2.1.

Table 2.1 Geometrical parameters of the Quattro robot and of its workspace.

Symbol	***Values [mm]***
a	275
b	375
c	825
d	75
e	780
f	220
g	200
h	700
m	1140
p	30.8

Let $\{x_0, y_0, z_0, \theta_0\}^{\mathrm{T}}$ be the end-effector pose, and $\{\varphi_1, \varphi_2, \varphi_3, \varphi_4\}^{\mathrm{T}}$ the active joint coordinates. In order to compute the performance indexes for the studied family of parallel manipulators, since the active joints are all rotational, the following formulation of the translational matrix $\boldsymbol{J}_{Dt}$ is used:

$$\boldsymbol{J}_{Dt}^{-1} = \boldsymbol{J}_q^{-1} \cdot \boldsymbol{D} \cdot \boldsymbol{J}_{xt} \tag{2.9}$$

Matrix $\boldsymbol{J}_q^{-1}$ is the inverse of the Jacobian matrix $\boldsymbol{J}_q$ and is defined as follows:

$$\boldsymbol{J}_q^{-1} = \begin{bmatrix} \frac{1}{j_{q_1}} & 0 & 0 & 0 \\ 0 & \frac{1}{j_{q_2}} & 0 & 0 \\ 0 & 0 & \frac{1}{j_{q_3}} & 0 \\ 0 & 0 & 0 & \frac{1}{j_{q_4}} \end{bmatrix} \tag{2.10}$$

with:

$$j_{q_i} = b\left[z_0 \cos\varphi_i + \left(a - x_0 - \frac{d\sqrt{2}}{2} - d\cos\left(\frac{\pi}{4} - \theta_0\right)\right)\sin\varphi_i\right] \quad (i=1,3)$$

$$j_{q_j} = b\left[z_0 \cos\varphi_j + \left(a - y_0 - \frac{d\sqrt{2}}{2} + d\sin\left(\frac{\pi}{4} - \theta_0\right)\right)\sin\varphi_j\right] \quad (j=2,4)$$

Matrix $\boldsymbol{J}_{xt}$ is the translational part of the Jacobian matrix $\boldsymbol{J}_x$ and is defined as follows:

$$\boldsymbol{J}_{xt} = \begin{bmatrix} x_0 + A + B - C_1 & y_0 + D - B & z_0 - E_1 \\ x_0 + A - B & y_0 + D + B - C_2 & z_0 - E_2 \\ x_0 - A - B + C_3 & y_0 - D + B & z_0 - E_3 \\ x_0 - A + B & y_0 - D - B + C_4 & z_0 - E_4 \end{bmatrix} \tag{2.11}$$

where:

$A = d\cos\left(\frac{\pi}{4} - \theta_0\right)$, $B = d\frac{\sqrt{2}}{2}$, $C_k = a + b\cos\varphi_k$, $D = d\sin\left(\frac{\pi}{4} - \theta_0\right)$, and $E_k = b\sin\varphi_k$ $(k=1,\ldots,4)$.

Finally, matrix $\boldsymbol{D}$ takes the following form: $\boldsymbol{D} = b \cdot \boldsymbol{I}_4$, where $\boldsymbol{I}_4$ is the identity matrix of size four and b is the crank length.

The DSI μ_ρ can be computed through the Eqs. (11), (12), and (13), by simply extracting the column vectors $\boldsymbol{J}_X^{-1}$, $\boldsymbol{J}_Y^{-1}$ and $\boldsymbol{J}_Z^{-1}$ from $\boldsymbol{J}_{Dt}^{-1}$:

$$\boldsymbol{J}_X^{-1} = \boldsymbol{J}_q^{-1} \cdot \begin{Bmatrix} x_0 + A + B - C_1,\ x_0 + A - B,\ x_0 - A \\ -B + C_3,\ x_0 - A + B \end{Bmatrix}^{\mathrm{T}} \cdot b \tag{2.12}$$

$$\boldsymbol{J}_Y^{-1} = \boldsymbol{J}_q^{-1} \cdot \begin{Bmatrix} y_0 + D - B,\ y_0 + D + B - C_2,\ y_0 - D \\ +B,\ y_0 - D - B + C_4 \end{Bmatrix}^{\mathrm{T}} \cdot b \tag{2.13}$$

$$\boldsymbol{J}_Z^{-1} = \boldsymbol{J}_q^{-1} \cdot \{z_0 - E_1,\ z_0 - E_2,\ z_0 - E_3,\ z_0 - E_4\}^{\mathrm{T}} \cdot b \tag{2.14}$$

2.3. Numerical Investigation on Adept Quattro™ robot

2.3.1. DSIs vs. manipulability

A numerical investigation has been carried out by applying the theory developed above to an industrial 4-RUU manipulator (the Adept Quattro). The goal of the investigation is to point out the different suggestions provided by the DSIs μ_X, μ_Y, and μ_Z and the manipulability indexes, in terms of regions of the workspace where the robot performances should be optimal. In order to achieve exhaustive predictions of the robot performances over its full workspace (shown in Fig. 2.2), it has been necessary to discretize the workspace through a regular and thick grid. The grid has been constructed by selecting 12 equally spaced horizontal planes, located at z_u ($u=1,...,12$) in the robot world reference frame. Half the planes belong to the upper cylindrical region of the workspace, half to the lower truncated conic region. Each plane contains 11 concentric circles of radius r_v ($v=1,...,11$). Each circle is split into 36 points with polar angle θ_w ($w=1,...,36$). Hence, the grind comprises 396 points spread through the entire volume of the workspace.

The cylindrical coordinates of each point P of the grid have been transformed into Cartesian coordinates in the robot world frame using the following basic expressions:

$$\begin{cases} x_P = r_v \cos\theta_w \\ y_P = r_v \sin\theta_w \\ z_P = z_u \end{cases} \tag{2.15}$$

The performance indexes in all the grid points have then been computed by setting $x_0 = x_P$, $y_0 = y_P$ and $z_0 = z_P$. The rotation of the end-effector (θ_0) has instead been set equal to zero in all the grid points.

Figures 2.3 through 2.8 show the values taken by the manipulability indexes μ_t (Fig. 2.3), μ_t^F (Fig. 2.4), μ_t^∞ (Fig.2.5) and by the DSIs μ_X (Fig. 2.6), μ_Y (Fig. 2.7), and μ_Z (Fig. 2.8) over the robot workspace.

In these figures a spatial view of the shapes of the indexes is given. So as to simplify the comparison among the predictions of the indexes, regardless of each index values and range of variation, the best performance regions take dark red color in all the figures, while the worst performance regions take dark blue color.

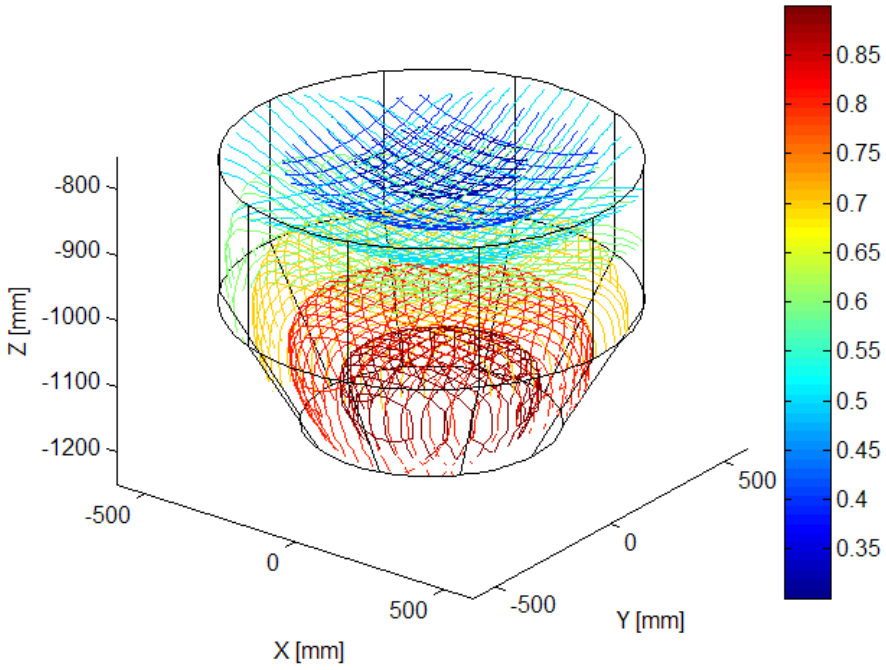

Fig. 2.3 Manipulability index μ_t .

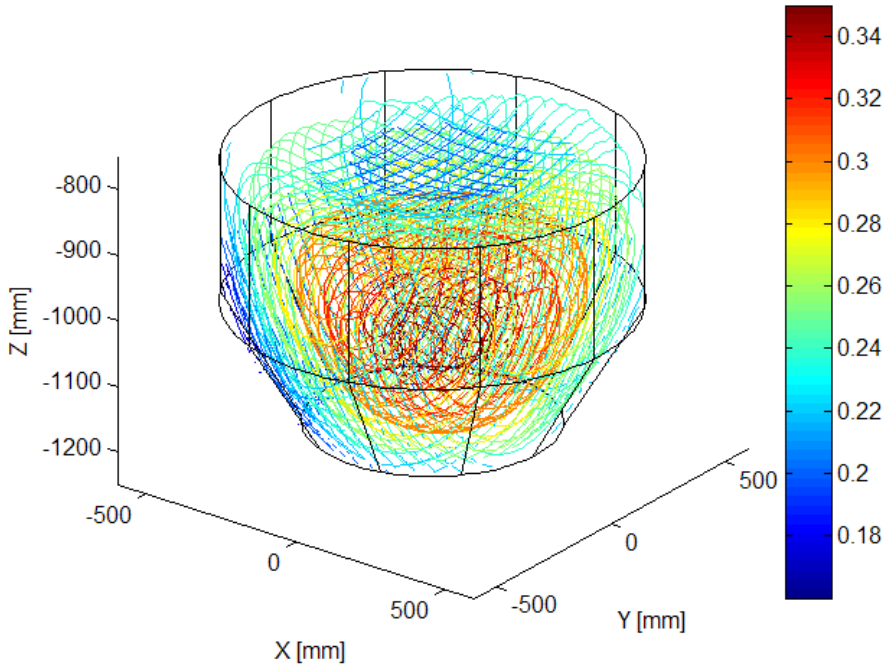

Fig. 2.4 Manipulability index μ_t^F.

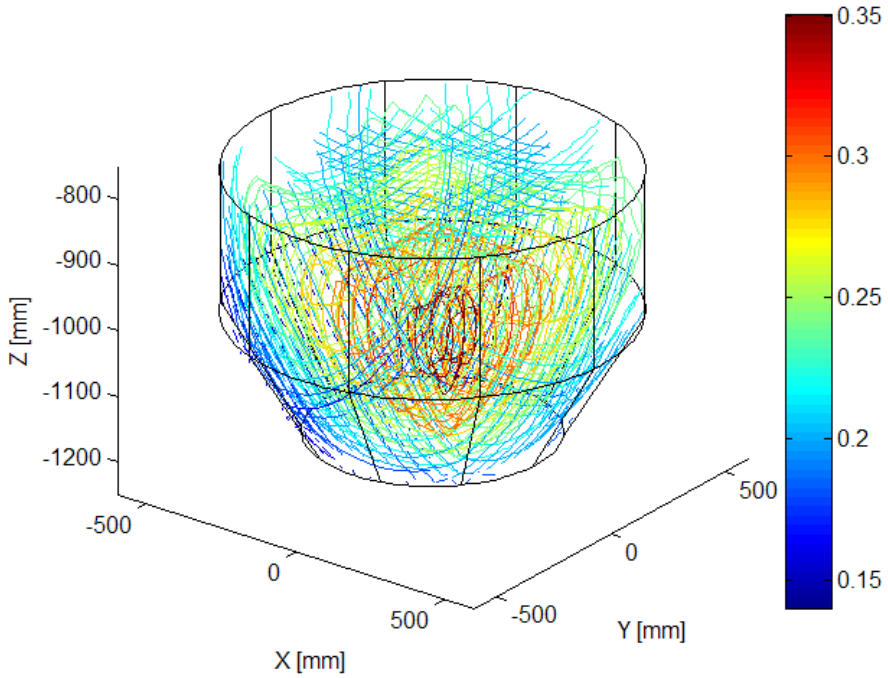

Fig. 2.5 Manipulability index μ_t^∞.

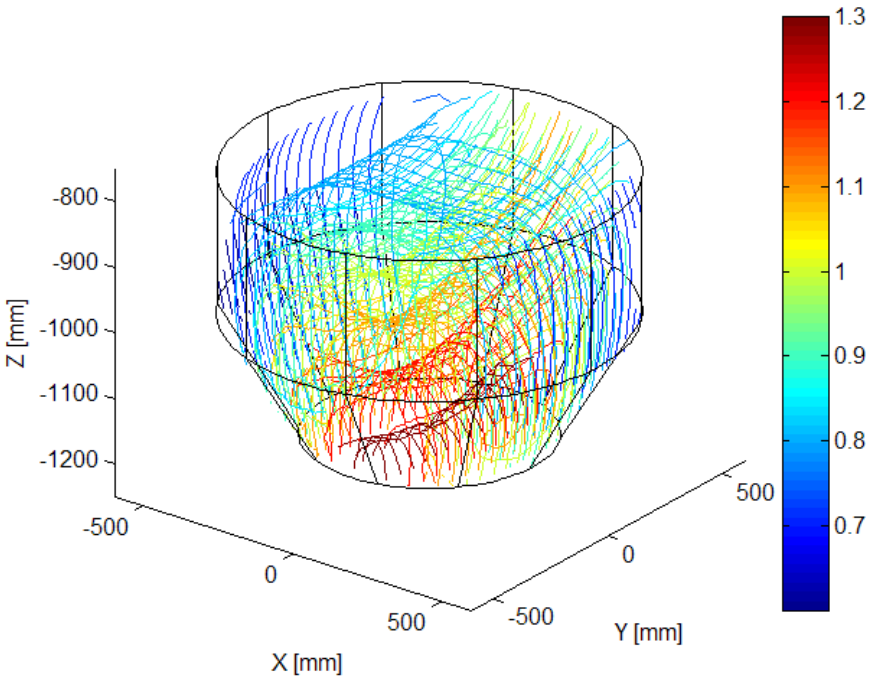

Fig. 2.6 DSI μ_X.

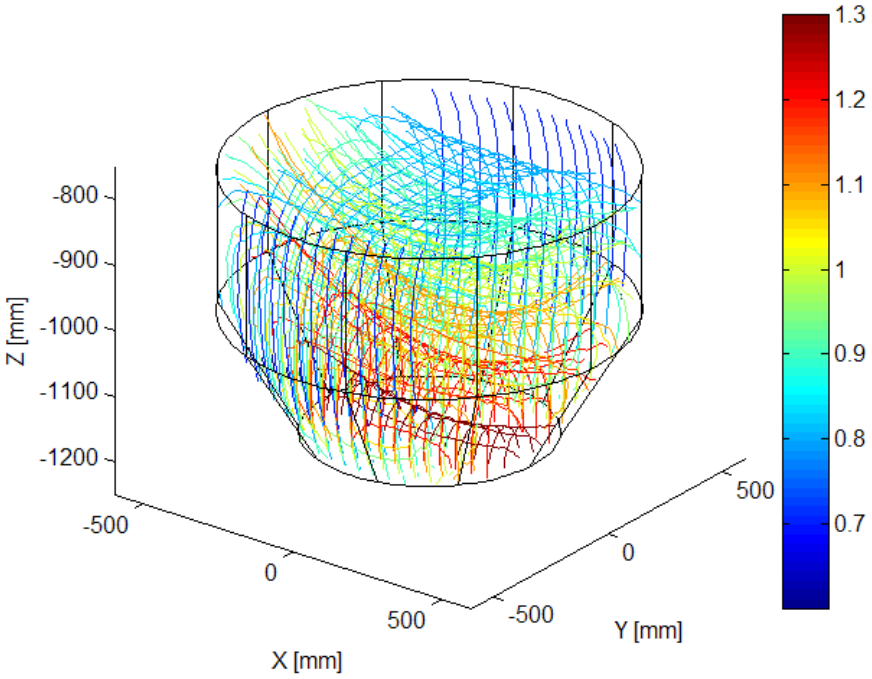

Fig. 2.7 DSI μ_Y.

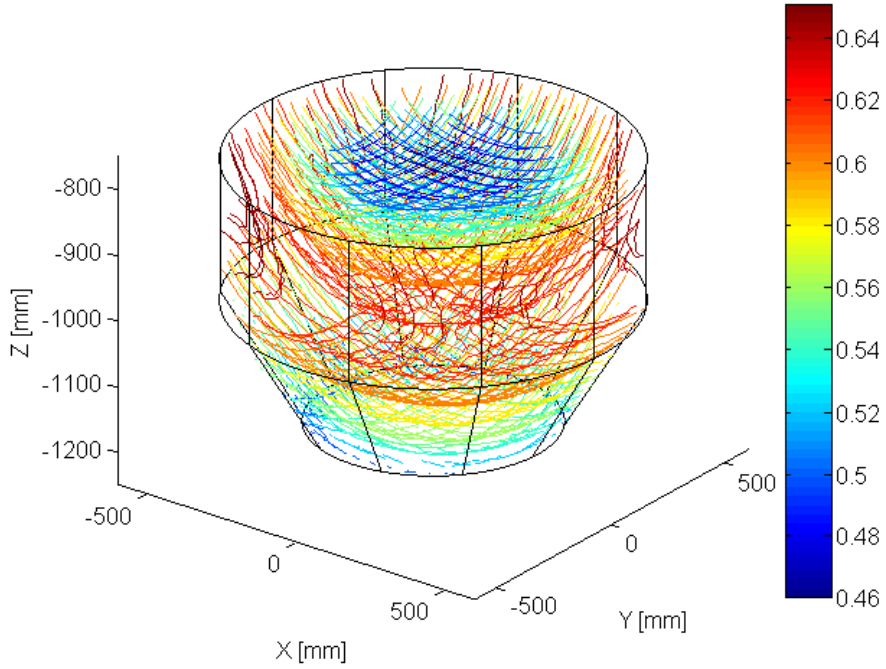

Fig. 2.8 DSI μ_Z.

It may be immediately recognized that the manipulability indexes μ_t, μ_t^F and μ_t^∞ have similar shapes: these indexes depict spherical-like and concentric isomanipulability surfaces. The indexes always take their best values in the inner regions of the workspace, which are hence identified as the best performance regions. The vertical position of such regions depends on the formulation chosen. The index values then decrease in the regions closer to the boundaries of the workspace. The shape shown by the manipulability indexes is rather intuitive: the best manipulator performances seems to be achievable close to the center of the manipulator workspace. However, considerably different hints comes from the DSIs μ_X, μ_Y, and μ_Z, i.e. when considering the expected performances for translations along different directions.

Let us first consider μ_X and μ_Y (Figs. 2.6 and 2.7), whose shapes are nearly identical, apart from a rotation by π/2 radians about the Z axis. The isomanipulability regions are no longer spherical-like and concentric, but rather half-oval in the best performance regions and elliptical-like elsewhere. Additionally, the best performance regions are not located at the center of the workspace but they are close to the boundaries and symmetrical across the axis orthogonal to the selected direction (e.g. orthogonal to axis *Y* in the case of μ_X, see Fig. 2.6). The worst performance regions are instead the ones which are furthest from the symmetry axis.

As far as μ_Z is concerned, Fig. 2.8 shows that the best values of the index are found in a ring-like region surrounding the upper part of the workspace. Less satisfactory values are instead computed for the lower part of the workspace.

A better understanding of the shapes of these indexes can be obtained by plotting the values they take on some significant sample planes. A few examples are shown in the figures from 2.9 through 2.13, where isomanipulability curves are shown. These figures allow highlighting better the differences between DSIs and manipulability. Since the shapes of the three manipulability indexes are alike (see Figs. 2.3, 2.4, and 2.5), and are very different from the ones of the DSIs, in the following analyses and figures only the manipulability index μ_t will be compared with the DSIs.

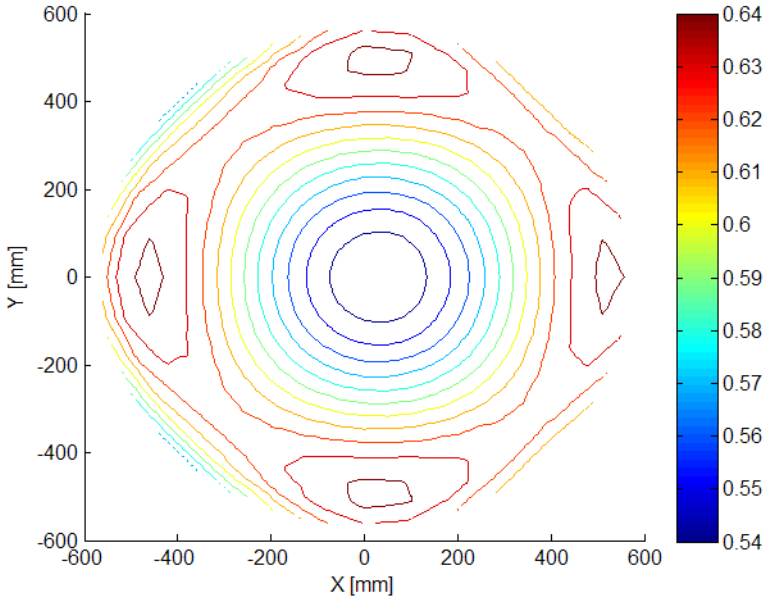

Fig. 2.9 Manipulability index μ_t in the *XY* plane (*Z*=-900).

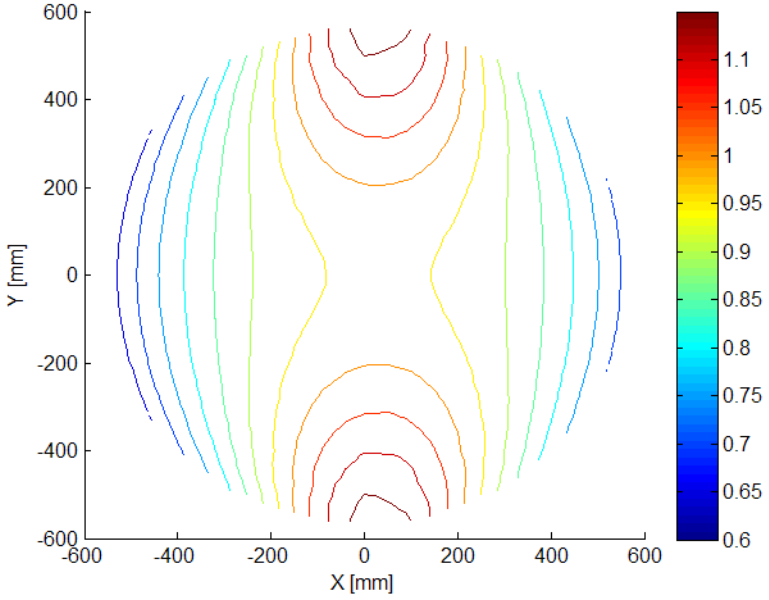

Fig. 2.10 DSI μ_X in the *XY* plane (*Z*=-900).

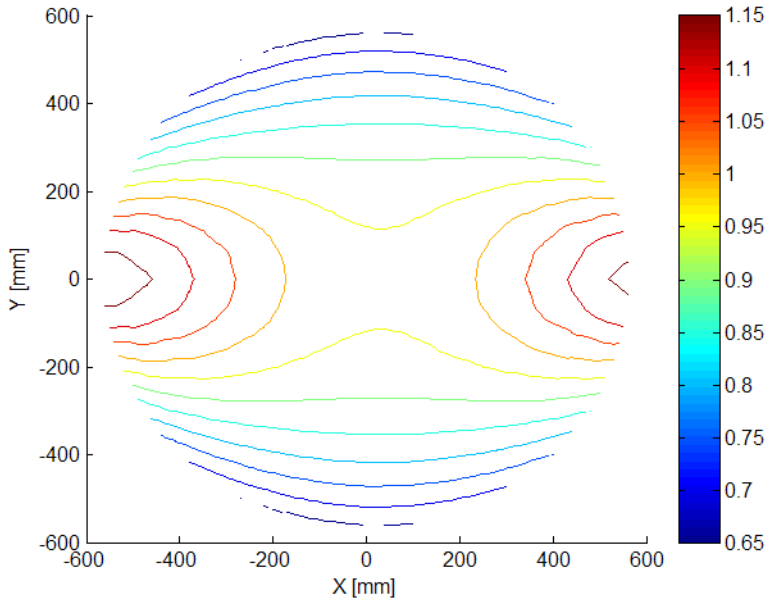

Fig. 2.11 DSI μ_Y in the *XY* plane (*Z*=-900).

Figures 2.9, 2.10, and 2.11 show the values taken in the *XY* plane with coordinate *Z*=-900 by the manipulability index μ_t, and by the DSIs μ_X and μ_Y. Such figures clarify the abovementioned differences between the best performance region predictions. It is apparent that the use of μ_t seems to lead to conclusions that are in misleading: for example the existence of four best performance regions rotated π/2 radians with respect to each other, is in contrast with the results provided by the DSIs, where two best performance regions rotated π with respect to each other appears close to the workspace boundaries and symmetrically displaced across the direction orthogonal to the selected direction of motion.

The values taken in the *YZ* plane with coordinate *X*=0 by μ_t, and by the DSI μ_Z are instead plotted in Figs. 2.12 and 2.13. The manipulability index μ_t (Fig. 2.12) reaches its best values in a region located close to the middle of the axis *Y*, and close to the bottom (i.e. to low values of *Z*) of the this planar slice of the

workspace. The manipulability values decrease in the areas close to the boundaries of the workspace and take the less satisfactory values at the top of the workspace.

Conversely, Fig. 2.13 shows that μ_Z takes its best values in a curved region crossing the planar slice of the workspace and achieving the very best values at the upper right and left boundaries. The region close to the bottom of workspace is where the less satisfactory values are computed.

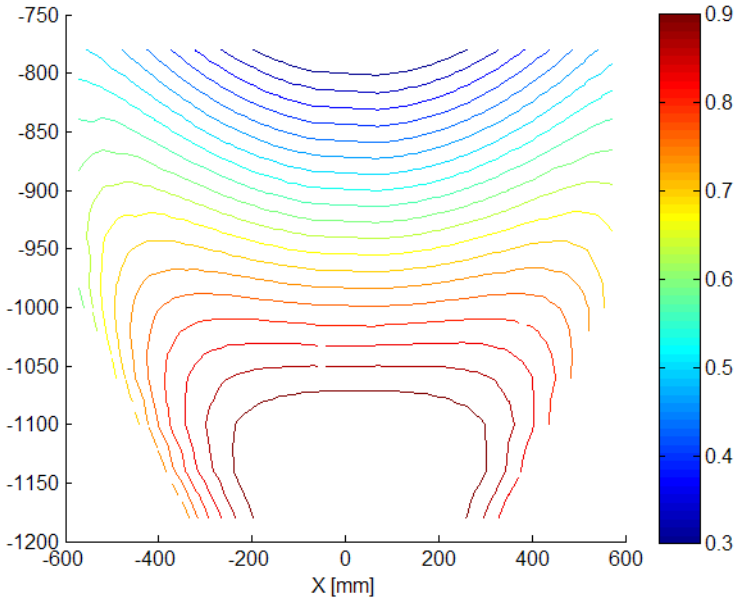

Fig. 2.12 Manipulability index μ_t in the *YZ* plane (*X*=0).

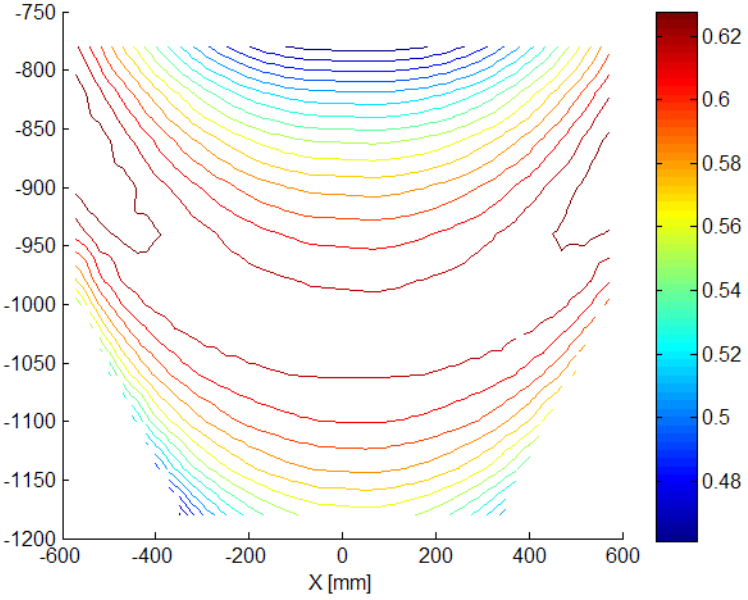

Fig. 2.13 DSI μ_Z in the *YZ* plane (*X*=0).

2.4. Experimental Validation

2.4.1. DSIs for displacements parallel to the three main axes

The numerical results shown demonstrate that there are significant discrepancies between the predictions made by manipulability indexes and the DSIs. In order to assess experimentally which indexes provide the best predictions, some relevant experimental tests have been carried out on the Adept Quattro manipulator.

The experiments have been carried out with two objectives:

- evaluating the velocity performances of the robot moving platform within the workspace

- verifying whether any comparison can be made between the measured performance variations and the predictions inferred by the indexes analyzed.

The moving platform of the Quattro robot has been instrumented with an uniaxial PCB MEMS accelerometer model 3741 (see Fig.2.14) alternatively employed to measure accelerations along the X and the Z axes of the robot world reference frame (see Fig.2.1). The adopted accelerometer has a measuring range of ± 30 G and a frequency range between 0 (DC) and 2 kHz. An HBM MGC signal conditioner with ML10 modules has been used to power the MEMS accelerometer and to filter its output signals (a low-pass filter having a Butterworth characteristic and a cut-off frequency of 200 Hz has been employed). The filtered data have been acquired and logged by means of an LMS Pimento analyzer. Finally, experimental data have been processed (high-pass filtered and integrated numerically) and compared to the performance index values using Matlab-Simulink.

The experimental tests have been carried out performing several repetitions of either straight horizontal displacements or straight vertical displacements in all the grid points into which the workspace has been split, and where performance indexes have already been computed.

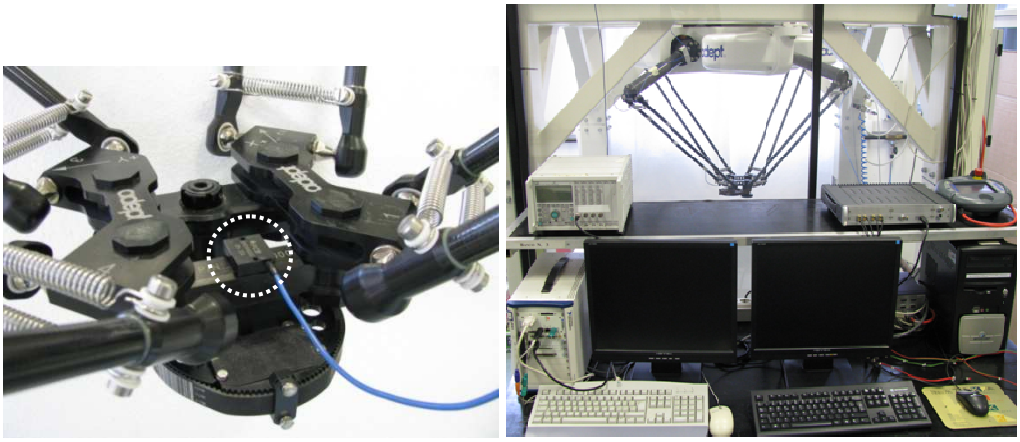

(a) (b)

Fig.2.14 (a) The MEMS accelerometer (in the dotted circle) fixed on the moving platform. (b) The experimental setup.

As far as the Adept V+ software program written to run the robot is concerned, it is worth highlighting that:

- the “continuous path” feature of the robot controller has been disabled to avoid modifications of the desired path during the manipulator motion;
- the “speed” command has been set equal to 100% (i.e. no speed limitation has been introduced in path planning);
- the sharpest acceleration profile (square-wave) has been adopted.

As far as the horizontal (along the X direction) displacements are concerned, around each grid point the end-effector has been made perform a sequence of six 30 mm straight forward displacements and five 30 mm straight backwards displacements. The peak-to-peak amplitude of the displacements is 60 mm. The midpoint of these displacements coincide with the grid point considered. The repetition of identical displacements has been motivated by the need of checking the repeatability of the measured accelerations.

Similar tests have been carried out with vertical displacements (along the *Z* direction): at each grid point the robot TCP has been made perform a sequence of six 30 mm straight upwards displacements and five 30 mm straight downward displacements. The peak-to-peak amplitude of the displacements is again 60 mm, and the midpoint of these displacements coincide with the grid point considered.

The acceleration data collected during the tests have been processed in order to gather the maximum horizontal and vertical velocity achieved by the robot TCP at each grid point. Maximum velocities are necessarily reached at the midpoints of the displacements (i.e. at the grid points of interests). As previously mentioned, velocities have been computed from accelerations by numerical integration. Signal detrending has been obtained by filtering the acceleration signals through a second order Butterworth highpass filter with passband frequency at 0.2 Hz.

A sample plot of the horizontal velocities computed is shown in Fig. 2.15. The same figure also shows the displacements computed through double integration: the mentioned 60 mm peak-to-peak amplitude of the displacements can be recognized. By comparing the two plots it can be also verified that maximum velocities are reached at about the mid points of the paths. The same considerations hold for the vertical velocities (see Fig 2.16).

For each direction of motion (horizontal or vertical) and for each sequence of displacements (i.e. for each grid point), the very maximum absolute value of velocity achieved during the repetition of the displacements has then been detected and related to the grid point. For example, the values computed for the points belonging to the horizontal half-plane *XY* at *Z*=-900 mm and to the vertical plane *YZ* at *X*=0 mm are plotted respectively in Fig. 17 (b) and in Fig. 18 (b) (at the

bottom of the figures). Velocity values have been normalized in order to take 1 as the maximum value.

Figures 17 and 18 also show the values taken by the studied performance indexes in the same planes: manipulability index μ_t is shown in Figs. 17 (a) and 18 (a), the DSIs μ_X and μ_Z are shown in Figs. 17 (c) and 18 (c) respectively.

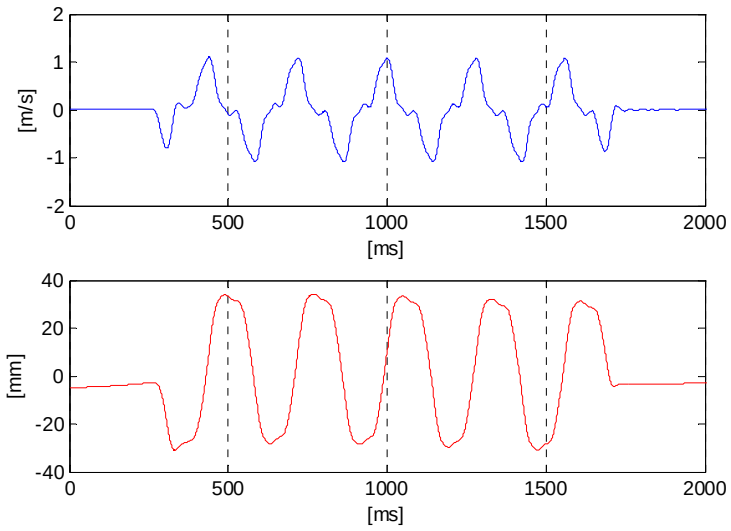

Fig. 2.15 Sample horizontal velocities and displacements of the robot TCP measured at a grid point of the workspace.

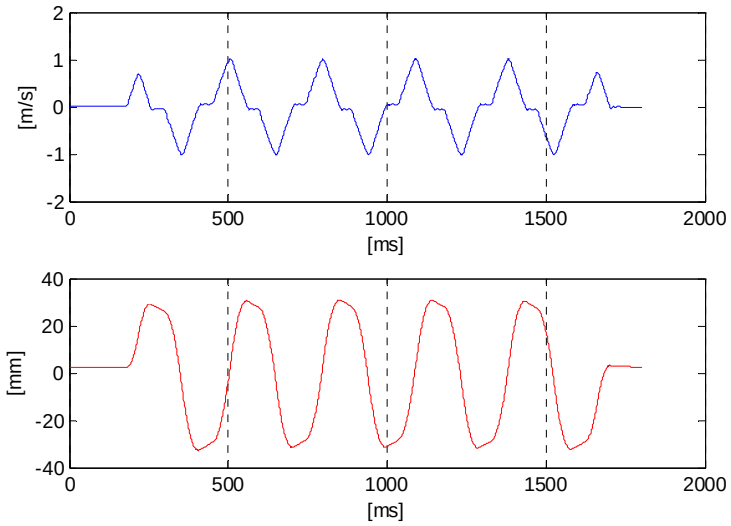

Fig. 2.16 Sample vertical velocities and displacements of the robot TCP measured at a grid point of the workspace.

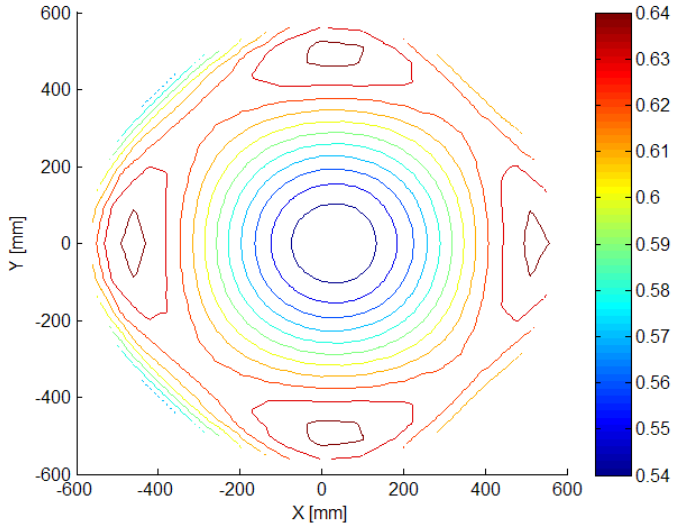

(a)

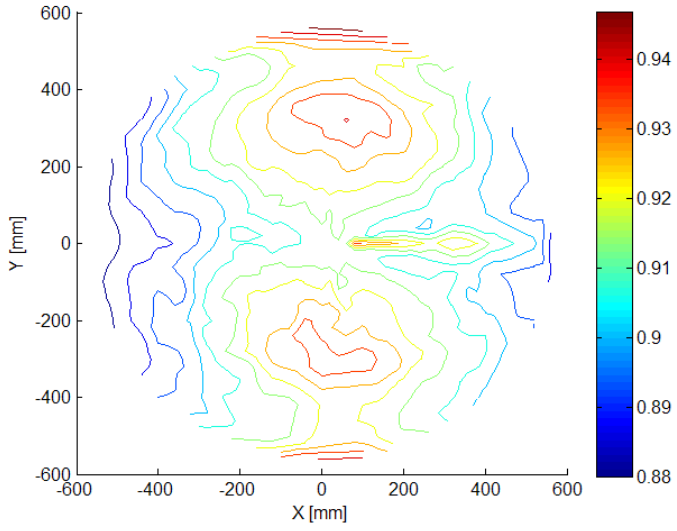

(b)

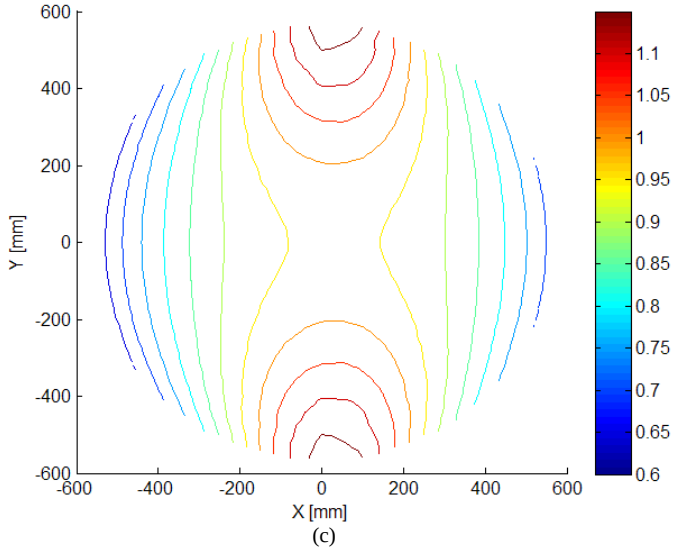

(c)

Fig. 2.17 Manipulability index μ_t (a), normalized velocity along the *X* direction (b), and DSI μ_X computed in the horizontal plane *XY* (*Z*=-900) (c).

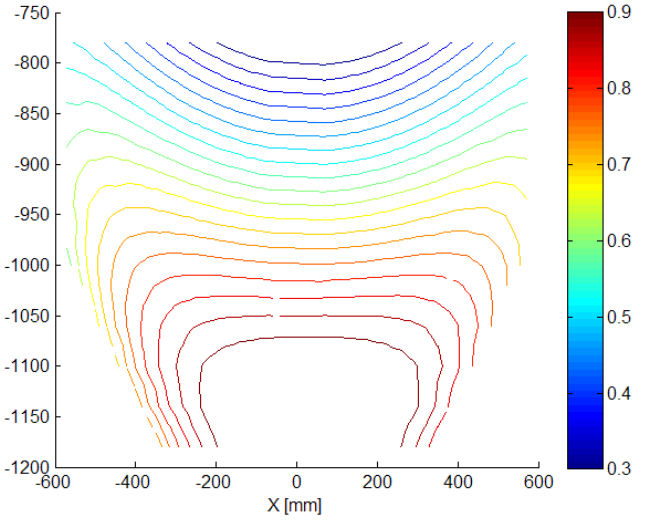

(a)

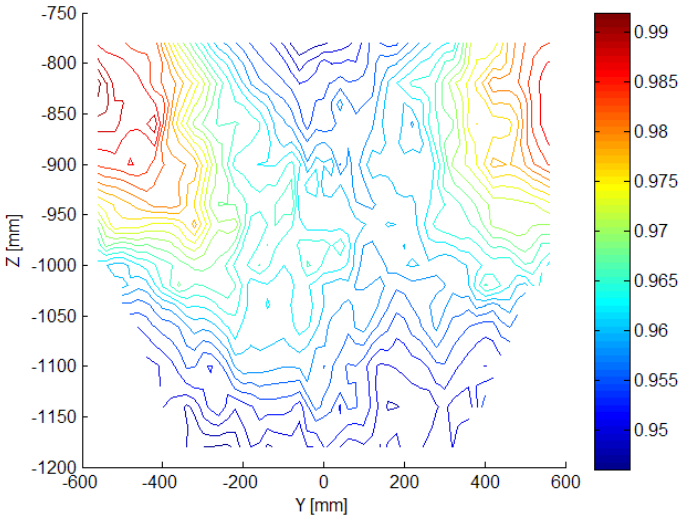

(b)

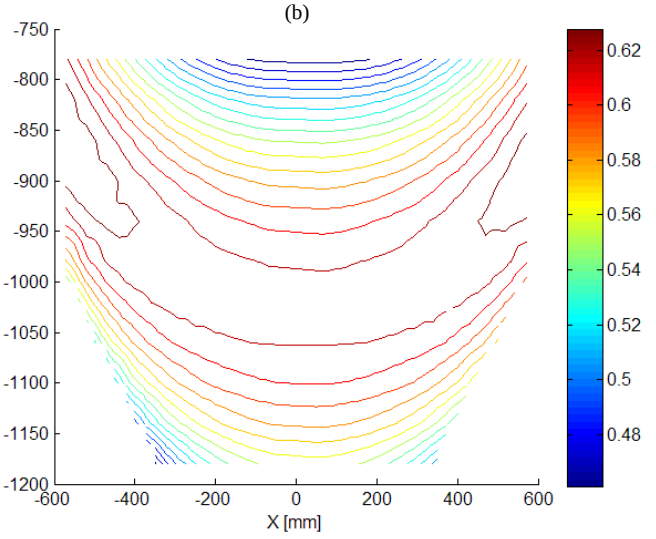

(c)

Fig. 2.18 Manipulability index μ_t (a), normalized velocity along the Z direction (b), and DSI μ_Z computed in the vertical plane YZ (X=0) (c).

It can be immediately recognized that in both cases the proposed DSIs μ_X and μ_Z show shapes very similar to the normalized maximum velocities. Not only do the best performance regions predicted by the DSIs fit well with the experimentally recorded data, but the performance variations foreseen by DSIs seem to be in good agreement with the recorded velocity variations. What is more important, the predictions provided by DSIs are considerably more accurate than the predictions provided by the manipulability index μ_t, which, in the case of horizontal displacements (Fig. 2.17), suggests four inexistent best performance regions, and in the case of vertical displacements (Fig. 2.18), completely misses the best performance region locations.

As final evidence of the usefulness of the suggested DSIs, in the figures from 2.19 through 2.22 μ_t, μ_X, and μ_Z have been related to the normalized maximum velocities achieved at each grid point of the vertical and horizontal planes shown in Figs. 2.17 and 2.18. Generally speaking, though the definitions of the adopted indexes are purely kinematic, it would be informative for good performance indexes to provide satisfactory estimates of dynamic performance variations within the workspace. In other words, a performance index would be practically useful if, for example an increase of the robot velocity could be predicted through a corresponding increase of the performance index. Figures 2.19 and 2.21 show that this is not the case when manipulability is considered: there seems to be no meaningful correlation between μ_t, and the TCP velocities in the horizontal and vertical directions. On the contrary, Figs. 2.20 and 2.22 prove that data are less scattered when the DSIs μ_X and μ_Z are considered: a satisfactory correlation appears between the DSIs and the velocity values.

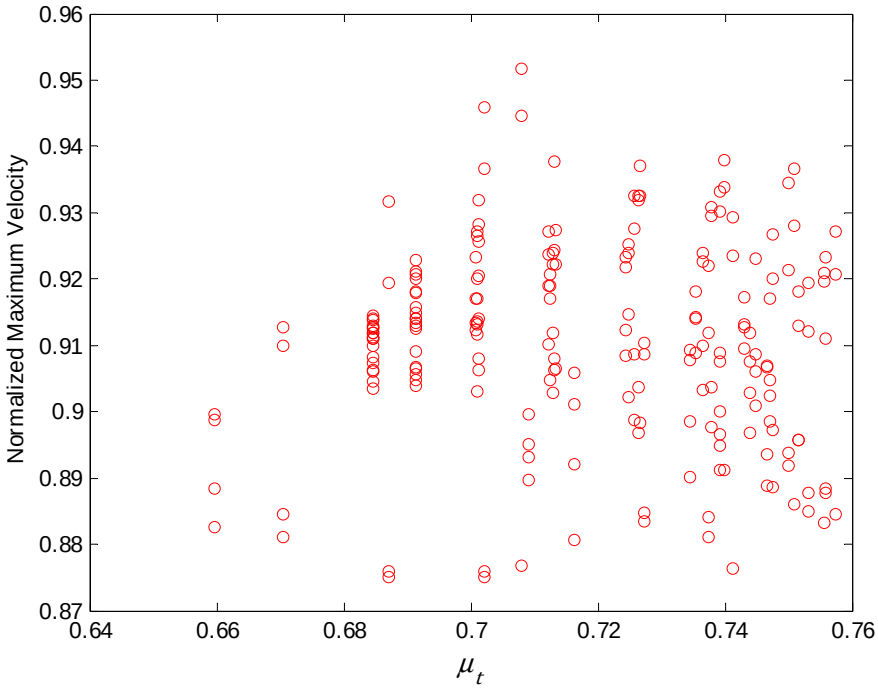

Fig. 2.19 Scattered diagram of manipulability μ_t vs. velocity along the *X* direction.

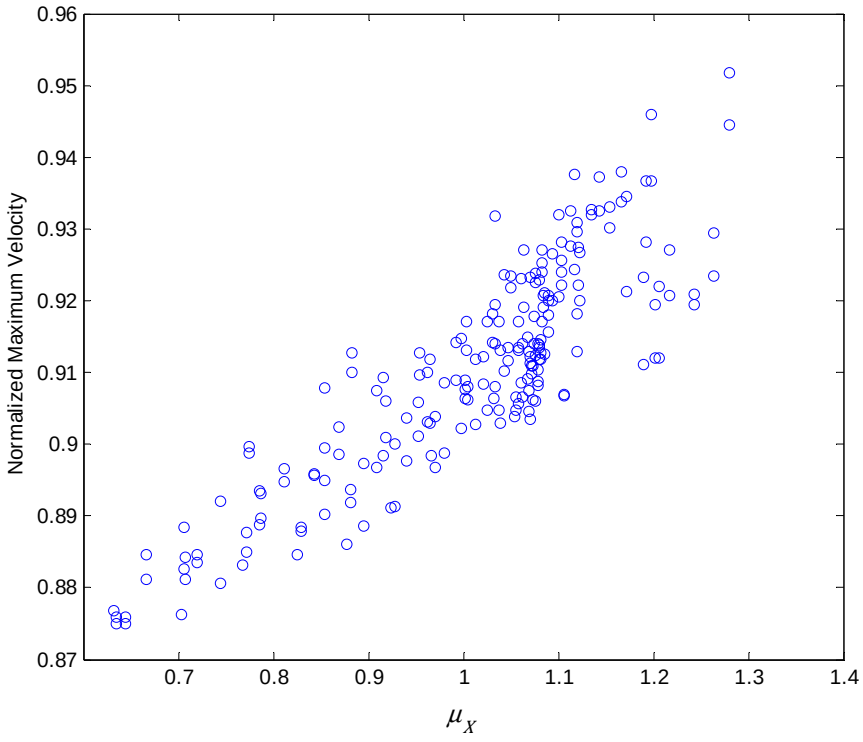

Fig. 2.20 Scatter diagram of DSI μ_X vs. velocity along the *X* direction.

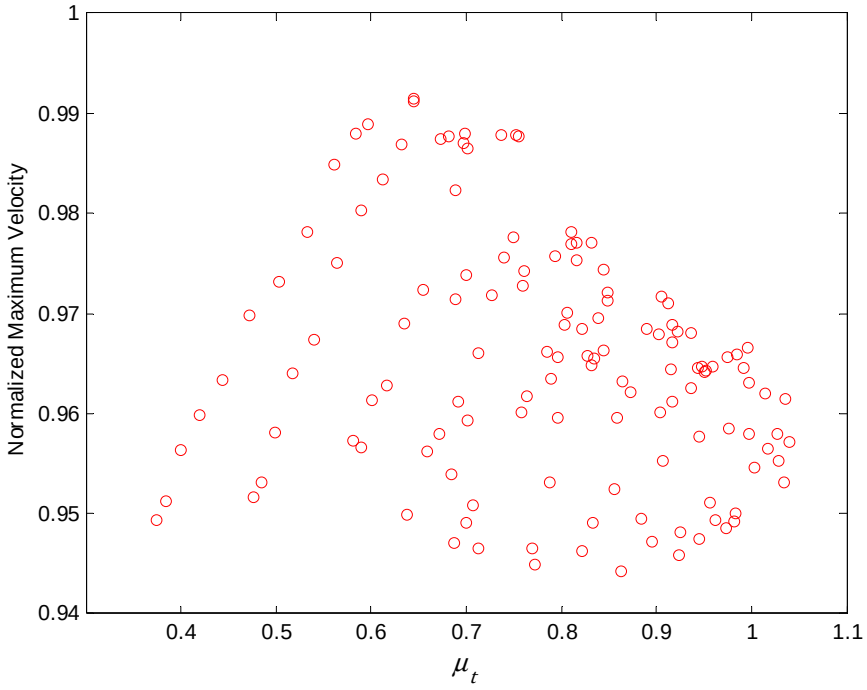

Fig. 2.21 Scattered diagram of manipulability μ_t vs. velocity along the Z direction.

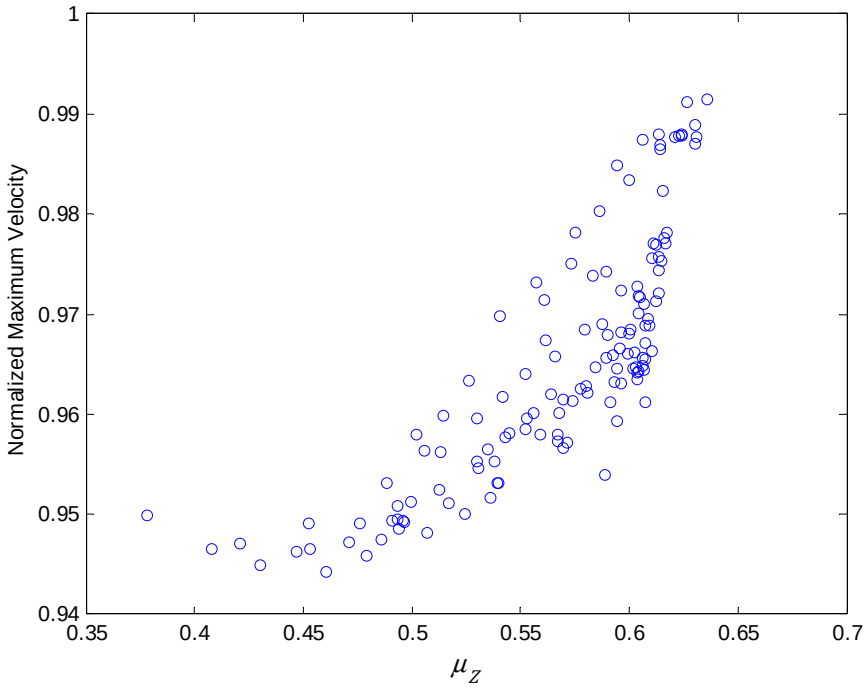

Fig. 2.22 Scatter diagram of DSI μ_Z vs. velocity along the Z direction.

2.4.2. DSIs for displacements along a generic direction

In the following experimental campaign the acceleration of the robot TCP has been measured by two uniaxial DC accelerometers (one PCB model 3741 with measuring range ± 30 G and frequency range DC-2 kHz, and one PCB model 3711 with measuring range ± 2 G and frequency range DC-350 Hz). Absolute acceleration has been computed as the resultant vector of the acceleration components detected along the two orthogonal measurement directions of the DC accelerometers (see the accelerometer mounting locations in Fig. 2.23).

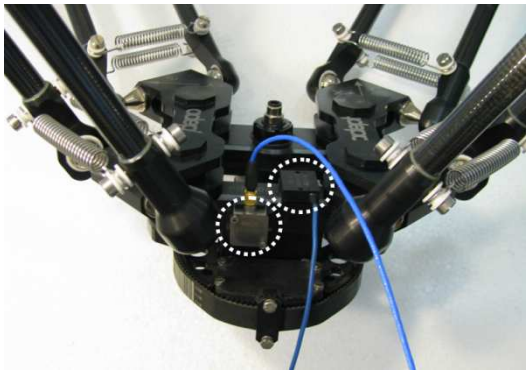

Fig. 2.23 The DC accelerometers (in the dotted circles) fixed on two orthogonal surfaces of the moving platform.

The workspace has been discretized through the same regular and thick grid of 4752 points presented in subsection 2.4.1. At each grid point the robot TCP has been made perform a sequence of five 30 mm straight forward displacements along a selected direction and five straight backwards displacements along the same direction. The peak-to-peak amplitude of the displacements is 60 mm. The midpoint of these displacements coincide with the grid point considered.

The features of path, speed and trajectory planning adopted in the experiments of subsection 2.4.1 have been used in this investigation.

The very maximum velocity achieved during the repetition of the displacements has been associated to the grid point and compared to the μ_R value computed at the same points using Matlab-Simulink.

Figures 2.24 and 2.26 show isolines of μ_R referred to two different directions (discussed below), while Figs. 2.25 and 2.27 show the normalized velocities recorded along the same directions. The velocity values have been normalized in the sense that they take 1 as the maximum value. The isolines have been obtained by interpolating the values referred to the 396 grid points belonging to the plane.

In particular, Figs. 2.24 and 2.25 refer to displacements in the horizontal plane *XY* at z_4=-900 mm and along directions parallel to the X_R axis of the reference frame obtained rotating about the *Z* axis by $\alpha = 70°$ the world reference frame. In such a case, the rotational matrix $\boldsymbol{R}$ takes the following simple form: $\boldsymbol{R} = \boldsymbol{R}_z(\alpha) \coloneqq \begin{bmatrix} \cos\alpha & -\sin\alpha & 0 \\ \sin\alpha & \cos\alpha & 0 \\ 0 & 0 & 1 \end{bmatrix}$.

In Fig. 2.24 it can be seen that the best performance regions (bordered by the lines in darker colors which are related to higher μ_R values) have approximately an half-oval shape and are located close to the workspace boundaries, symmetrical across the axis orthogonal to the selected direction. Similar results have been obtained experimentally: by comparing Fig. 2.24 with Fig. 2.25 it can be noticed that the performance variations foreseen by μ_R are in good agreement with the normalized velocity variations recorded at the same grid points.

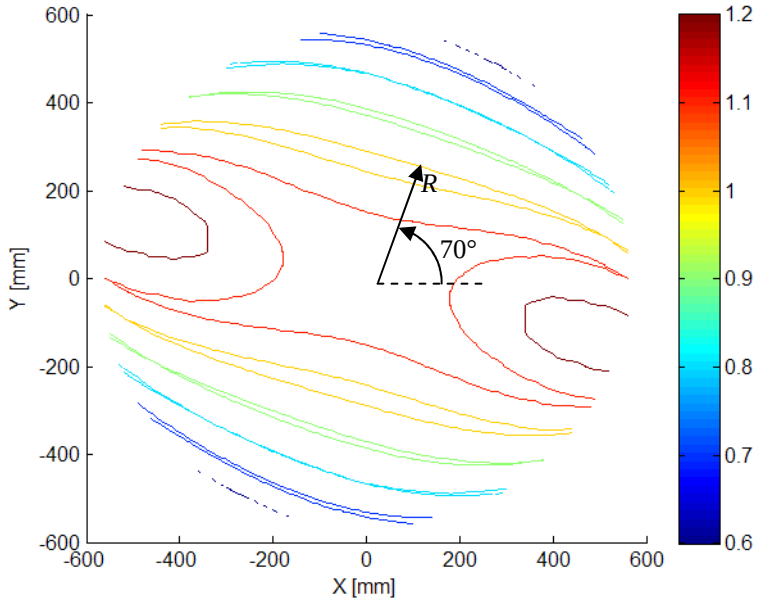

Fig. 2.24 μ_R along the direction R in the horizontal (XY) plane with z_4=-900 mm.

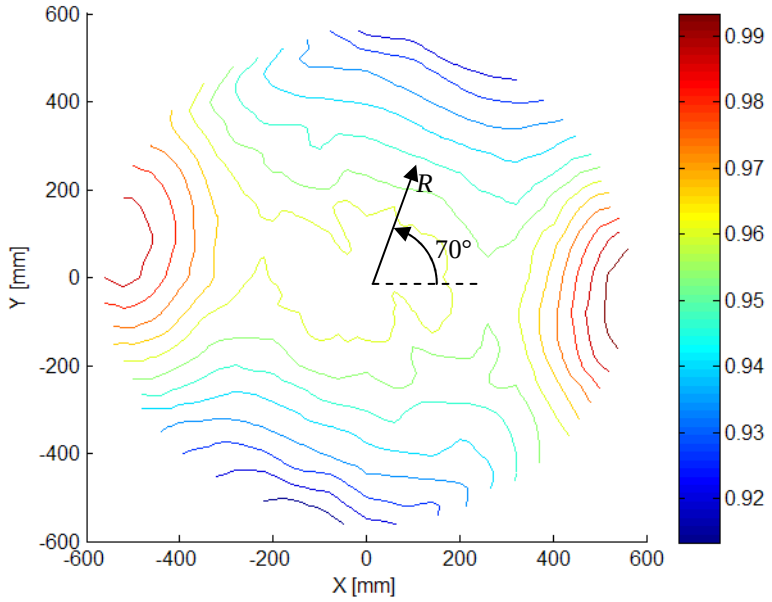

Fig. 2.25 Normalized velocities along the direction R in the horizontal (XY) plane with z_4=-900 mm.

A second comparison between index predictions and recorded velocities is proposed in Figs. 2.26 and 2.27. It refers to displacements along the direction taken by the X_R axis when the reference frame (X_R, Y_R, Z_R) is rotated by an angle $\beta = -70°$ about the *Y* axis of the world reference frame. Hence, matrix $\boldsymbol{R}$ takes the form $\boldsymbol{R} = \boldsymbol{R}_y(\beta) \coloneqq \begin{bmatrix} \cos\beta & 0 & \sin\beta \\ 0 & 1 & 0 \\ -\sin\beta & 0 & \cos\beta \end{bmatrix}$. Direction *R* lies in the XZ plane, hence only its projection R_x on the XY plane is shown in the Figs 12 and 13.

In detail, Fig.2.26 shows the μ_R isolines computed in the horizontal plane (*XY*) at z_4=-900 mm. μ_R reaches its best values in a region bordered by red color lines located close to the right boundary of the planar slice of the workspace and takes the less satisfactory values on the opposite part of the plane. The isolines inferred from the normalized velocity values recorded at the same grid points are shown in Fig. 2.27. Again, it can be recognized that the different performance regions predicted by the DSI fit well with the experimentally recorded data: the DSI isolines show shapes very similar to the ones of the normalized maximum velocities.

In conclusion, the comparison among the values of DSIs manipulability, and the normalized maximum velocities experimentally recorded performing horizontal and vertical movements in a large number of points has demonstrated that DSIs can better foresee the best performance regions within the workspace and that the performance variation predictions made through the DSIs are in good agreement with the recorded velocity variations.

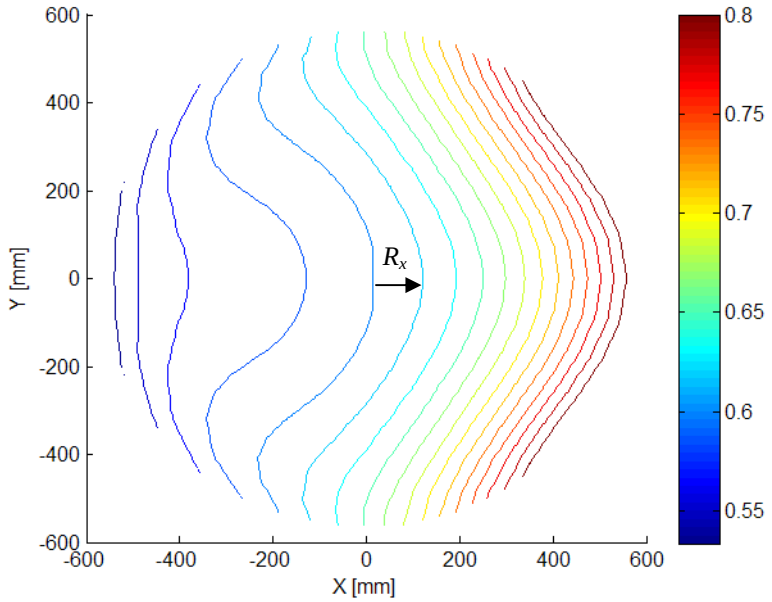

Fig. 2.26 $\mu_R$along the direction *R* in the horizontal (*XY*) plane with z=-900 mm.

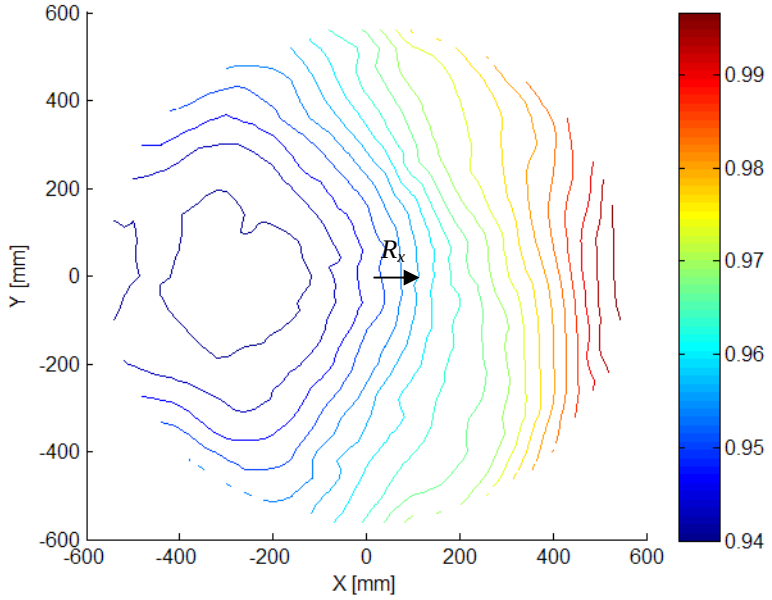

Fig. 2.27 Normalized velocities along the direction *R* in the horizontal (*XY*) plane with z=-900 mm.

3 TASK DEPENDENT PERFORMANCE INDEX (TPI) AND OPTIMAL ROBOT POSITIONING

3.1. TPI analytical formulation

The proposed TPI index is task dependent in the sense that the index computation takes into account the sequence of movements to be accomplished by the robot to carry out a complete task.

In order to infer the general TPI formulation, let us consider a generic robotic task from a start point (sp) to an end point (ep) whose path comprises a series of straight-line segments l_i connected by via points (vp_j), as depicted in Fig. 3.1 (a).

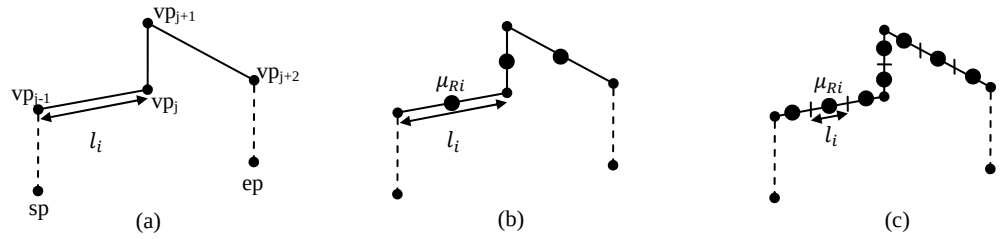

Fig. 3.1 The path related to a generic task (a). The same path split into a series of segments (b) or sub-segments (c).

Generally speaking, when uncoupled DSIs are available for horizontal and vertical movements, they may be usefully adopted to foresee performances on those tasks (e.g. the pick-and-place task), which consist of continuous sequences of vertical and horizontal displacements.

Once the directions of the path segments are known, a single DSI (μ_{Ri}) can be computed at each *i*-th segment midpoint: see Fig. 3.1 (b). Afterwards, on the basis of the length l_i of each *i*-th segment of the path, the weighted average of all the DSIs along the path can be computed. The weights are computed by comparing the lengths of the segments to the total length of the task path. Such an average leads to the following TPI definition:

$$\text{TPI} = \frac{\sum_{i=1}^{n} \mu_{Ri} \cdot l_i}{\sum_{i=1}^{n} l_i} \tag{3.1}$$

where *n* is the number of segments into which the path is split.

More accurate TPI values can be achieved by further splitting the segments into sub-segments of either identical or dissimilar length (see Fig. 3.1(c)). At each sub-segment midpoint it is possible to compute the DSI value and then replicate the averaging procedure leading to TPI computation.

It is important to underline that the analytical TPI expression in Eq. (3.1) is invariant with respect to the choice of the fixed reference frame and can be used to evaluate the performance of a robot in a specific task of interest. Additionally, as it is discussed below, it can be usefully employed to determine the optimal relative position between a robot and an assigned task.

3.2. Numerical investigation on Adept Quattro™ robot

In order to validate the effectiveness of the proposed TPI index and to show its straightforward applicability to parallel robot optimal positioning, the theory above has been applied to the execution of a pick-and-place task by the industrial parallel robot Adept Quattro™.

The tasks evaluated are pick-and-place ones, which are very popular in industry, and in particular in the typical fields of application of parallel robots, such as assembly and packaging operations, palletizing, loading and unloading of conveyor belts, etc.

Pick-and-place operations are commonly related to a path which takes the shape depicted in Fig. 3.2: it consists of a first straight vertical motion at the pick-up location (from the starting point sp to the via point vp_1), followed by a straight horizontal motion (from vp_1 to vp_2) and by another straight vertical motion at the placement location (from vp_2 to the end point ep). The lengths of the three straight segments are denoted respectively by L_{v1}, L_h, and L_{v2}; L_{v1} and L_{v2} are often identical.

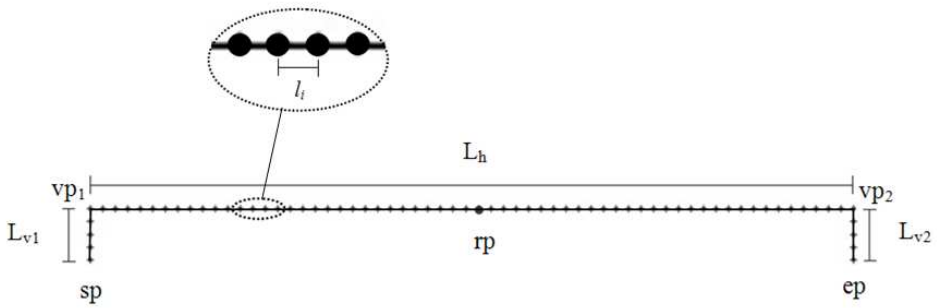

Fig.3.2 The pick-and-place task path and its main geometrical parameters.

Figure 3.2 also shows the location of the reference point rp associated to the path. Since the task path is symmetrical, the midpoint of the sequence of movements is the preferred choice for placing rp.

Table 3.1 collects the total length (L_{tot}) of the pick-and-place path considered in this investigation, as well as the lengths of its segments (L_{v1}, L_h, and L_{v2}) and of the sub-segments (l_i) into which it has been split. Indeed, so as to apply the TPI definition in Eq. (3.1), the pick-and-place task path has been split into 71 sub-segments characterized by an equal length l_i (see the representation in the oval in Fig. 3.2). Such a length has been selected in order to have a significant number of segments leading to an accurate TPI estimation.

Table 3.1 Lengths of the pick-and-place path, of its segments and sub-segments.

Symbol	***Values[mm]***
L_{v1}	25
L_h	305
L_{v2}	25
L_{tot}	355
l_i	5

The whole workspace has been considered for the optimal relative positioning between the task and the robot, clearly, in case of additional constraints (e.g. introduced by obstacles), a subset of the workspace could be considered.

In order to achieve exhaustive predictions of the robot performances over its full workspace, it is necessary to discretize the workspace through a regular and thick grid. Therefore the workspace has been discretized through the same regular and

thick grid of 4752 points presented in subsection 2.4.1. The reference point of the pick-and-place path has been made coincide with each gridpoint in order to find the best relative positioning between the robot and the task. Such an operation has also allowed checking whether or not the path can be entirely executed keeping the robot TCP within the workspace. Hence a realistic mapping of the robot performances has been achieved: the points at which the task could not be executed have been neglected.

In detail, two pick-and-place tasks have been considered in two separate investigations:

- Test 1: a pick-and-place task carried out with the longest segment of the path parallel to the *X* axis of the world reference frame;
- Test 2: a pick-and-place task carried out with the longest segment of the path parallel to the *Y* axis of the world reference frame.

Though in each test a complete path is defined (according to the scheme in Fig. 3.2), it makes sense investigating whether DSI and TPI provide similar or different predictions of the best performance regions. Clearly, DSI computation can only be done along a single direction and is in no relation with the length of the displacements. The much higher ratio L_h/L_{tot} than L_{v1}/L_{tot} or L_{v2}/L_{tot} makes computing the DSI along the longest segment (i.e. the horizontal direction) the most reasonable choice to try comparing DSI an TPI performance predictions. However it is also informative observing the predictions provided by the DSI computed along the direction of the shortest segments (i.e. the vertical direction).

Figures 3.4 (a) and 3.5, 3.6 (a) and 3.6 (b) show the results of such a comparison in, respectively Test 1 and Test 2. In particular, Fig. 3.5 shows the TPI values computed over the robot workspace. Figure 3.4 (a) shows instead the DSI values μ_X computed for translations along the *X* axis of the world reference frame). The best performance regions are those in dark colors, while the worst ones are in light colors.

Let us consider the isomanipulability regions of μ_X in Fig. 3.4 (a). The best performance regions according to the DSI are close to the lower workspace boundaries and symmetrically displaced across the vertical plane translated by *p* from the *YZ* plane with coordinate *x*=0 in *X* positive direction and orthogonal to the direction of the longest task segment (L_h). The worst performance regions are instead identified as the ones which are furthest from the just mentioned plane of symmetry.

The best performance regions for the TPI in Fig.3.5 are not located as the ones of μ_X but appear in the inner upper part of the workspace and placed near the vertical axis of the robot reference frame. These also are symmetrical across the vertical plane translated by *p* from the *YZ* plane with coordinate *x*=0 in *X* positive direction and orthogonal to the selected direction (e.g. orthogonal to the direction parallel to axis *Y* in the case of TPI for displacements parallel to the *X* axis).Moreover the TPI takes its worst values in the region closed to the upper part of the workspace and then in the lower part.

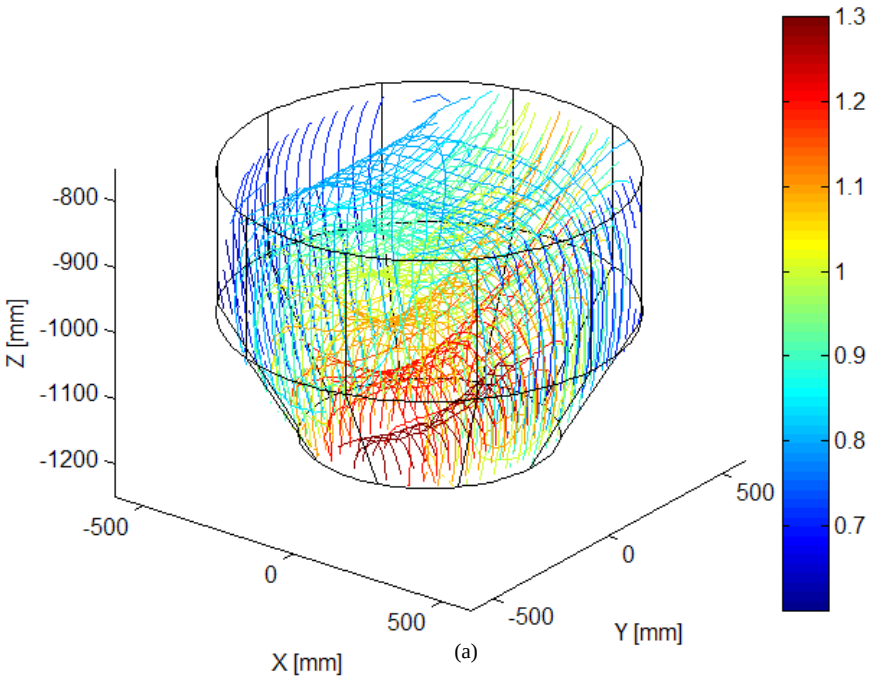

(a)

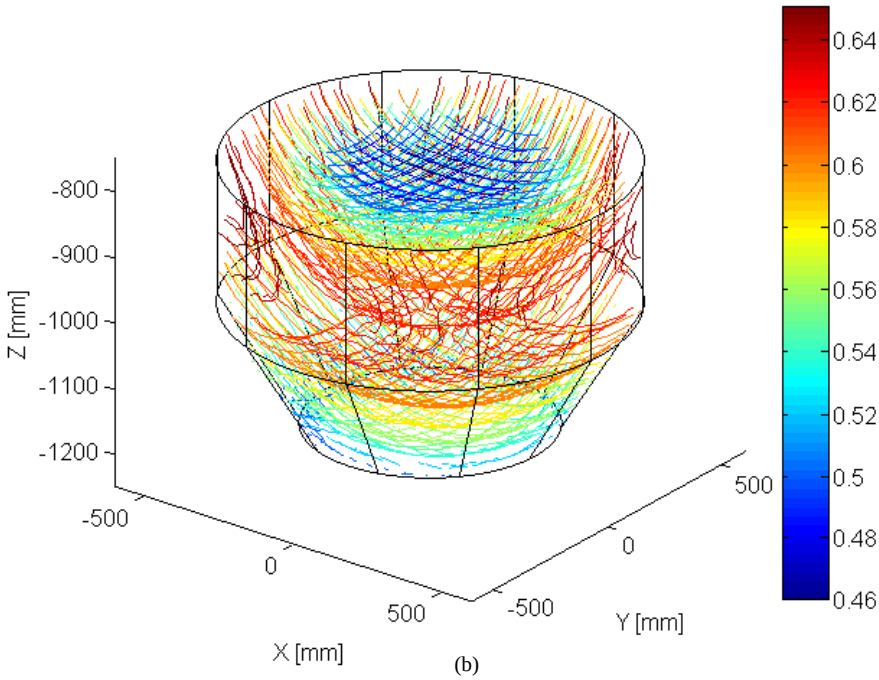

(b)

Fig. 3.4 DSI μ_X (a) and DSI μ_Z (b).

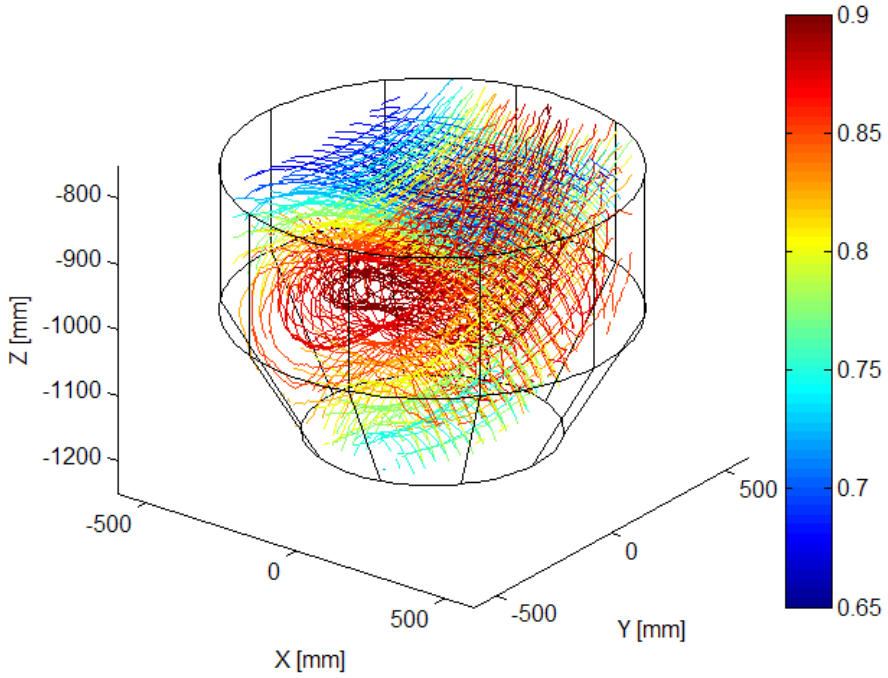

Fig. 3.5 TPI in Test 1

It is apparent that the use of TPI seems to lead to conclusions that are in contrast with the results provided by the μ_X. In fact, for calculating DSI, its definition is applied to the reference point and only considering the direction of the longest segment of pick-and-place. While the TPI definition taking into account the entire sequence of movements, hence the direction and geometry not only of the horizontal trait of pick-and-place task but also of the vertical ones. As a consequence, both μ_X and μ_Z values influenced the TPI computation and the location of the best performance regions. Therefore it is important to understand how the robot performances change within the robot workspace in executing more complex tasks than a single translation. As far as μ_Z is concerned, Fig.3.4 (b) shows that the best values of the index are found in a ring-like region surrounding

the upper part of the workspace. Less satisfactory values are instead computed for the lower part of the workspace.

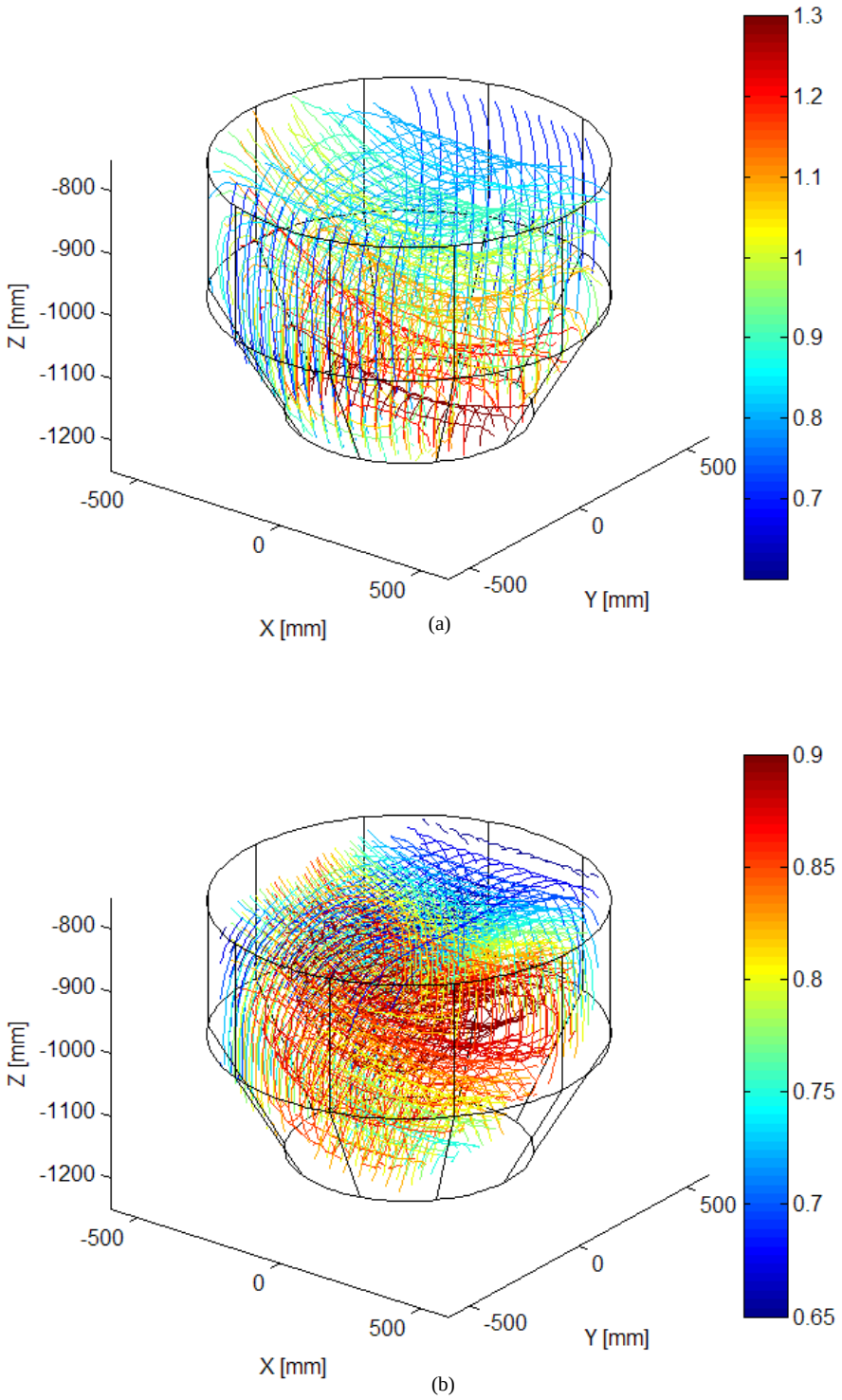

Fig. 3.6 Test 2. DSI μ_Y (a) vs. TPI (b).

Similar considerations for Test 1 can be drawn for the investigation carried out in Test 2, whose results are collected in Fig.3.5: Fig. 3.5 (a) shows the DSI values over the robot workspace $\mu_Y$while Fig. 3.5 (b) shows the TPI values. The shapes of the DSIs and TPIs in Test 2 are nearly identical to the ones in Test 1 apart from a rotation by $\pi/2$ radians about the *Z* axis. This is due the choice of the direction along which the sequence of translations are carried out. In fact, the longest segment of path is parallel to the *Y* axis of the world reference frame with obviously a difference of $\pi/2$ radians from the direction studied in the Test 1, where the pick-and-place task is instead carried out with the longest segment of the path parallel to the *X* axis. Moreover in Test 2 the plane of symmetry is no longer the one in Test 1, but it is the vertical *XZ* plane with coordinate *y*=0. As seen in Test 1, also in Test 2, μ_Z values with μ_X ones influenced the TPI computation. Since for μ_Z the values computed over the robot workspace are the same of Fig.3.5, such a figure is not repeated in this comparison.

In conclusion, the numerical investigation has proved an expected result: TPI, though being based on DSI, can provide performance predictions that differ significantly from those of any DSI employed in the computation. This is a consequence of both using DSI in the TPI formulation and explicitly considering the length and direction of the sequence of translations into which the task path can be split.

Hence, two aspects need to assessed experimentally: the general meaningfulness of DSI predictions and the task-specific correctness of TPI predictions. These two issues have been addressed through the experimental validation discussed in Chapter 4.

4 OPTIMAL ROBOT/TASK RELATIVE POSITIONING BASED ON TPI MAXIMIZATION

4.1. Robot design optimization

Robot design optimization plays a crucial role in the ever-continuing effort to improve robot performances and increase their productivity. Several approaches have been proposed to address performance optimization problems, they usually focus on the following issues:

- optimization of the design configuration of a given manipulator ([GOSSELIN 1989], [MAYORGA 1997], [KHATAMI 2002], [MAYORGA 2005], [FATTAH 2002]),
- improvement of the workspace reachability in an environment with obstacles or maximization of the workspace volume ([CHEDMAIL 1996], [STAN 2008]),
- optimization of robot architecture by considering several criteria simultaneously ([STOUGHTON 1993], [STOCK 2003], [LI 2004]),
- optimization of the scheduling and the robot configuration for some task points in order to minimize the trajectory run time ([PETIOT 1998], [ZACHARIA 2005]),
- optimization of robot positioning (base placement) for prescribed tasks [MITSI 2008].

As far as the first approach is concerned, some researchers have addressed the optimization of the dexterity characteristic of a robot ([GOSSELIN 1989], [MAYORGA 1997]) or of kinematic isotropy ([KHATAMI 2002], [MAYORGA 2005], [FATTAH 2002]) in order to obtain an optimal design. A simple index based on the upper bound for a standard condition number of the Jacobian matrix has been proposed in [MAYORGA 1997] and applied to the kinematic design optimization of a planar redundant manipulator. In [KHATAMI 2002] a genetic algorithm has instead been developed by exploiting the Global Isotropy Index in order to find optimal link lengths of the best isotropic robot configurations at optimal end-effector working points. Some years later, in [MAYORGA 2005] another index has been derived from a homogenized isotropy condition of a properly weighted Jacobian matrix. A general criterion for kinematic design optimization has then be developed in order to identify the optimal design configuration of a given manipulator.

As previously mentioned, another chief robot characteristic which can be optimized is the workspace. Workspace highly affects the tasks to be performed, especially when the environment is complex, dense or cluttered. In [CHEDMAIL 1996] a genetic algorithm has been used to establish the base position and type of a manipulator optimizing workspace reachability in an environment with obstacles. Several years later, a genetic algorithm-based approach has been presented in [STAN 2008] for workspace optimization of six-dof parallel micro robots. The objective of such a study was to evaluate optimal link lengths which maximized the workspace. The effort towards workspace optimization makes sense mainly in

parallel robots which usually have a workspace volume smaller than the that of serial robots.

A few works also addressed the optimization problem by considering several criteria simultaneously ([STOUGHTON 1993], [STOCK 2003], [LI 2004]). In [STOCK 2003] an optimal kinematic design method suitable for parallel manipulators has been developed. The solution of such an approach is a design which represents the best compromise between manipulability and a new performance index, named space utilization, whose value reflects the ratio between workspace size and the physical size of the robot structure. Li and Xu in [LI 2004] developed a mixed performance index using the space utility ratio for kinematic optimization of manipulators. This index is a weighted sum of Global Dexterity Index and a space utility ratio: it is helpful in optimizing the architecture of parallel manipulators.

Other works have been focused on the concurrent optimization of robot scheduling and configuration: in some industrial operations. In these cases, a primary problem for robotized cell designers is the optimal scheduling of the task point order minimizing the task execution time. This problem is reminiscent of the classic Travelling Salesman Problem (TSP), but the quantity to be optimized is time instead of distance. A simultaneous research of the optimal scheduling and of the optimal choice of the configurations of the robot for each task point has been presented in [PETIOT 1998]. In order to minimize the trajectory run time of the robot the elastic net method (ENM) has been used which permits to minimize an energy function using a modified gradient method. Because of the considerable computer time cost it is very difficult to use such a method in the case of robots

with more than three degrees of freedom. A method based on genetic algorithms has instead been proposed in [ZACHARIA 2005] to determine the minimum cycle time of a manipulator visiting several task points exactly once. Both the task point visit order and the multiple solutions of the inverse kinematic problem are considered. Such an algorithm can be applied to any non-redundant manipulator with up to six-degrees of freedom.

Regarding the determination of the optimum base location of a robotic manipulator, a hybrid heuristic method has been presented in [MITSI 2008]. Such a method combines a genetic algorithm, a quasi-Newton algorithm and a constraints handling method.

This Chapter focuses on an optimization problem similar to the one tackled in [MITSI 2008]. In particular, it addresses the issue of seeking the optimal relative position between a robot and a generic task composed of an arbitrary sequence of straight line movements. The optimization problem is translated into the problem of selecting the relative position maximizing a suitably defined performance index, which explicitly accounts for both the robot kinematics and the task geometrical features. The performance index introduced in this work has been specifically developed for parallel robots (as all the indexes discussed in [MERLET 2006]) and represents an evolution and a generalization of the Direction Selective performance Index (DSI) first presented in [BOSCHETTI 2010]. DSI allows obtaining uncoupled evaluations of the horizontal and vertical translational capabilities of parallel robots along selected directions. So far the DSI definition has been restricted to directions coinciding with the axes of the world reference frame. In this work a more general definition is achieved (i.e. a definition holding for any

direction in the Cartesian space) and then employed to develop a task-dependent performance index, i.e. an index also accounting for the sequence of movements to be accomplished by the robot during the task.

Hence, there are two main motivations for this Chapter:

- Introducing a TPI-based method for optimal robot/task relative positioning.
- Proving the practical usefulness of the proposed method by means of experimental tests on a parallel robot.

As a proof of concept, the TPI formulation has been employed in a maximization algorithm in order to optimize the location of some pick-and-place tasks within the workspace of an industrial parallel robot. Such an algorithm has been implemented using Matlab. The industrial parallel manipulator considered is the Adept Quattro^{TM}, which belongs to the family of four-leg delta-like (4-RUU) manipulators.

4.2. TPI maximization algorithm for optimal robot positioning

The search for optimal robot/task positioning, i.e. the computation of the optimal relative position between a robot and a task to be carried out, can be translated into the problem of selecting the relative position maximizing the TPI related to the robot and the task assigned.

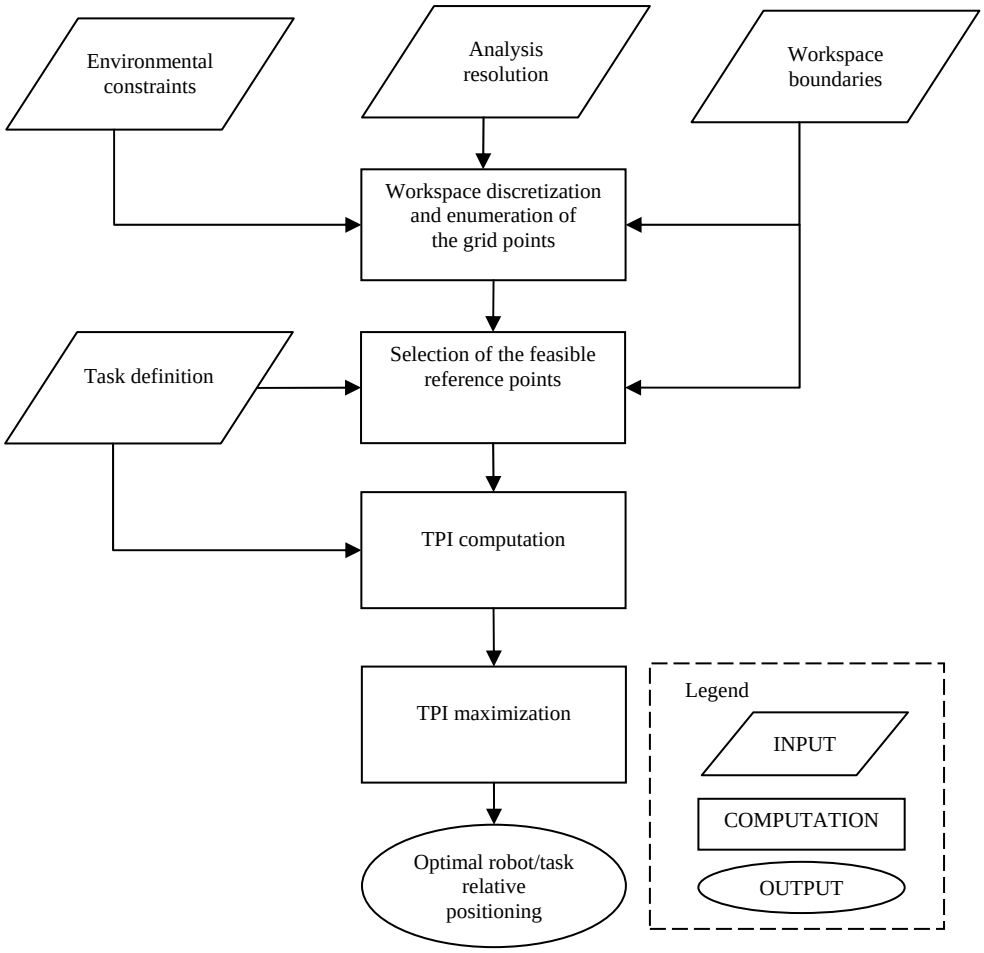

Fig. 4.1 Flow chart of the maximization procedure

A maximization algorithm/procedure exploiting the TPI formulation has therefore been developed. The procedure, represented in the flowchart in Fig. 4.1, assumes that the robot base is fixed while the task location is varied within the whole robot workspace in order to find the optimal location (or locations) where the task should be executed. In practice the result achieved by the algorithm is the optimal robot/task relative positioning, which can be exploited to either optimally locate the task within the robot workspace, or, if the task location cannot be modified, to identify the best robot base location within a workcell.

The data needed to execute the procedure can be summarized in the following three input parameter:

1. Workspace boundaries (defining the constraints of the robot reachable workspace).
2. Environmental constraints (caused, for example, by the presence of obstacles reducing the reachable workspace, or by production specifications).
3. Task definition (comprising the exact definition of the task path, of its reference point, and of the segments into which the path should be split for TPI computation).
4. Analysis resolution (i.e. how fine the workspace discretization should be)

The procedure consists in the following five steps:

- On the basis of inputs 1, 2 and 4 the workspace is discretized into grid points whose coordinates are computed and enumerated.
- Among all the grid points, those which can become feasible reference points are selected on the basis of inputs 1 and 3. A reference points is marked “feasible” if its task is completely retained within the workspace restricted by the environmental boundaries.
- TPI is computed at each feasible reference point.
- TPI maximization is performed and the reference point(s) with the highest value(s) of TPI is/are detected.

- The optimal robot/task reference position(s) is/are estimated as the position(s) where maximum TPI value(s) is/are achieved.

4.3. TPI experimental validation

Three independent sets of pick-and-place tasks have been carried out: two with the L_h segment parallel to the *X* axis of the world reference frame (Test 1 and Test 2), the other with the L_h segment parallel to the *Y* axis (Test 3). In Test 1 and 3 performance variations along vertical directions have been evaluated, while in Test 2 variations along an horizontal direction have been considered. In all the tests the analysis has been restricted to 21 points with each of which the path reference point has been made coincide during the experiments. In particular, in Test 1 and 3 such points belong to the *Z* axis and have the following Cartesian coordinates::

$$\begin{cases} (x_{\mathrm{rp}})_{\mathrm{k}} = 0 \\ (y_{\mathrm{rp}})_{\mathrm{k}} = 0 \\ (z_{\mathrm{rp}})_{\mathrm{k}} = \left(z_{\mathrm{rp}}\right)_1 - 20 * (k-1) \end{cases} \tag{4.1}$$

where $(z_{\mathrm{rp}})_1$ = -780 mm and k = 1, ..., 21. The subscript rp has been introduced to recall that these are the coordinates progressively given to the path reference point during the tests. In Test 4, instead, the Cartesian coordinates of the 21 points investigated are:

$$\begin{cases} (x_{\mathrm{rp}})_{\mathrm{k}} = (x_{\mathrm{rp}})_1 - 50 * (\mathrm{k} - 1) \\ (y_{\mathrm{rp}})_{\mathrm{k}} = 200 \\ (z_{\mathrm{rp}})_{\mathrm{k}} = -900 \end{cases} \tag{4.2}$$

where $(x_{\mathrm{rp}})_1$ = 500 mm and, once again, k = 1, ..., 21.

Spatial views of the 21 pick-and-place task paths related to each test are shown in Fig.4.2(a) for Test 1, in Fig.4.3(a) for Test 2, and in Fig.4.4(a) for Test 3. In Fig.4.3(a) some of the paths are drawn in dotted lines to show that those tasks cannot be executed, since at least one of their points does not belong to the workspace (whereas their reference points do). By referring to the algorithm described in paragraph 4.2, the reference points related to such paths are marked as unfeasible: in the enumeration they are the first and last sets of three reference points (i.e. those with k = 1, 2, 3 and k = 19, 20, 21). Conversely, Test 1 and 3 do not possess unfeasible reference points.

The TPI values computed in the XZ plane (Y = 0) for Test 1, in the XY plane (Z = -900) for Test 2, and in the YZ plane (X = 0) for Test 3 are depicted by means of isolines in, respectively, Fig.4.2(b), Fig. 4.3(b), and Fig.4.4(b). The isolines have been created by interpolating the values computed at the grid points belonging to the planes analyzed. The same figures also show the positions taken by the reference points during the tests.

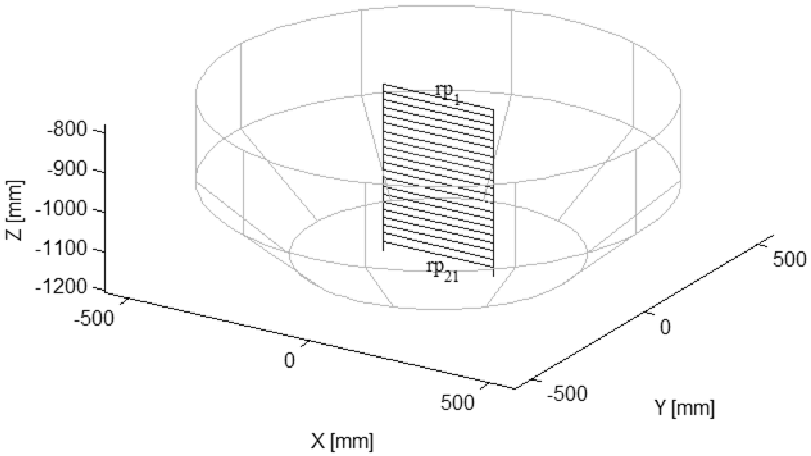

(a)

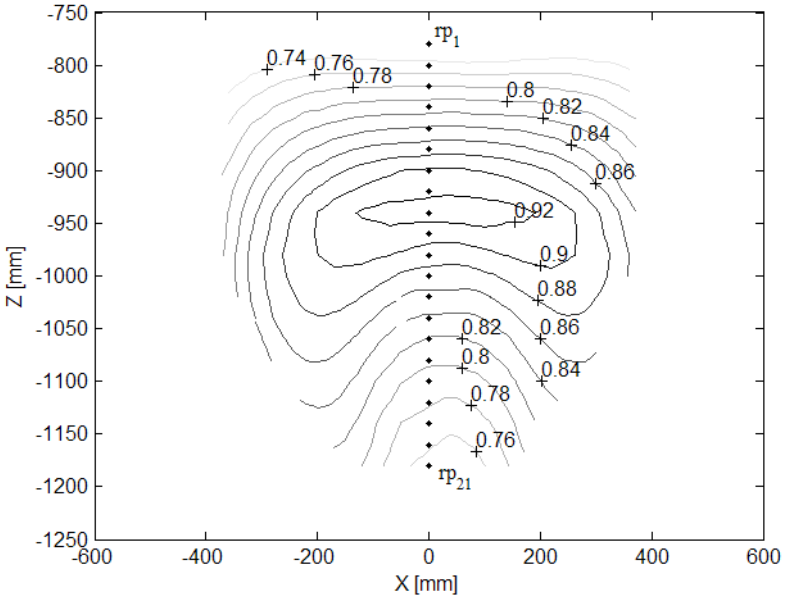

(b)

Fig. 4.2 Spatial view of the 21 task paths of Test 1 (a); TPI values and reference points positions(b).

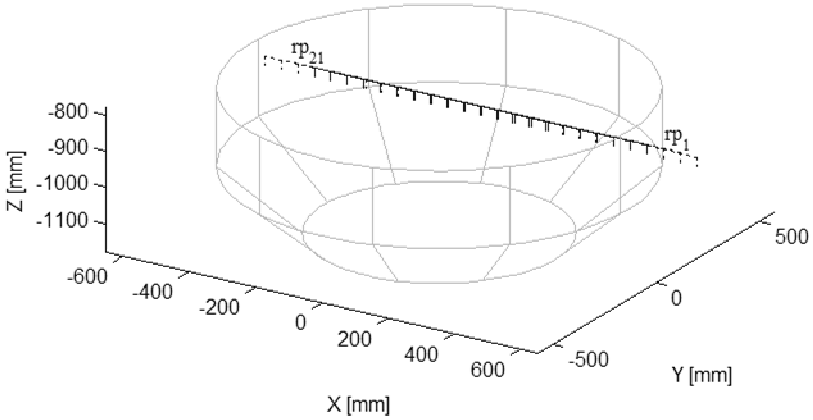

(a)

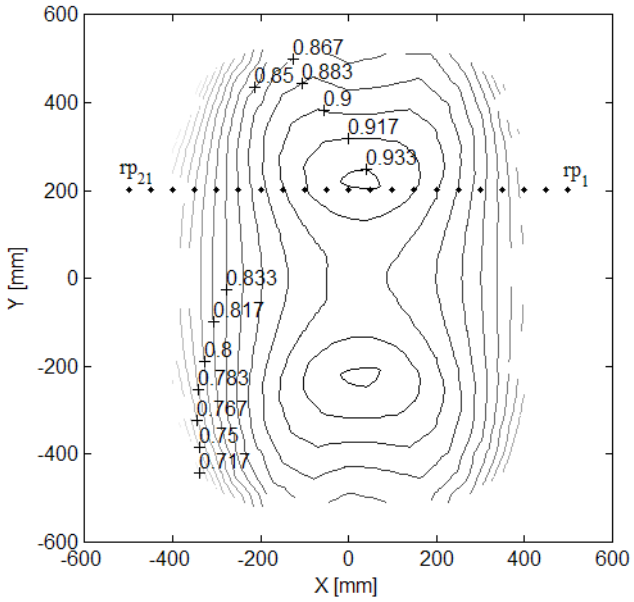

(b)

Fig. 4.3 Spatial view of the 21 task paths of Test 2 (a); TPI values and reference points positions (b).

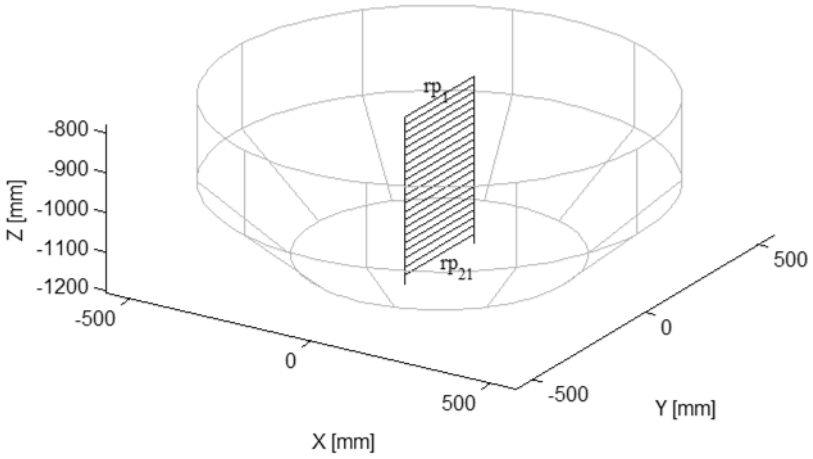

(a)

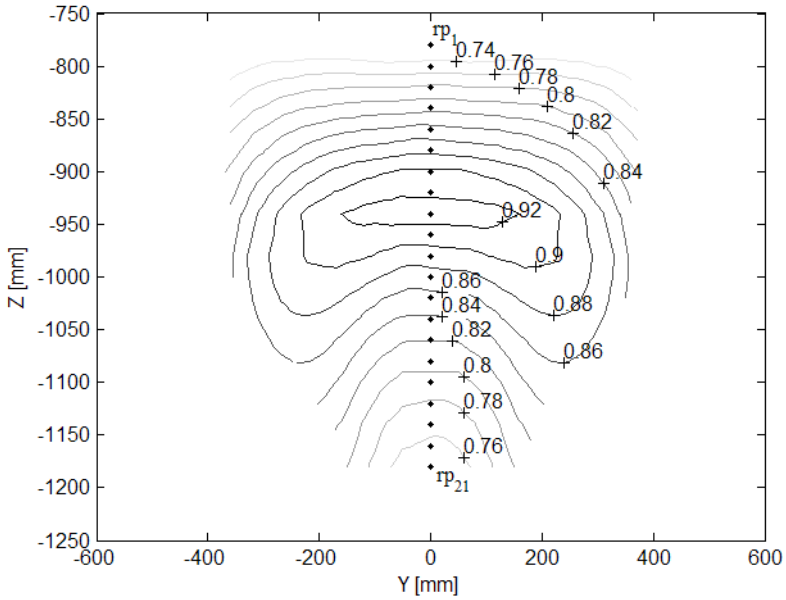

(b)

Fig. 4.4 Spatial view of the 21 task paths of Test 3 (a); TPI values and reference points positions (b).

In Fig. 4.2(b) it can be observed that TPI reaches its best values in the elliptical-like region bordered by the darkest color line close to the coordinate $z = z_5 = -940$ mm. Less satisfactory values are achieved above and below such a coordinate, the

worst being at the upper and lower boundaries. A similar shape of the TPI isolines can be noticed in Fig. 4.4(b), which refer to Test 3. Clearly, a different expected behavior can be recognized in Fig.4.3(b) for Test 2: two best performance regions with elliptical-like shape appear in the inner part of the robot workspace, along the *Y* axis. Lower TPI values characterize the areas closer to the workspace boundaries.

It should also be remarked that, as a straightforward consequence of the geometrical symmetry of the robot kinematic chains, the TPI isolines are symmetric with respect to the axis x=p in Test 1 (Fig. 4.2(b)), to the axes x=p and y=0 in Test 2 (Fig. 4.3(b)) and to the axis y=0 in Test 3 (Fig. 4.4(b)).

In Table 4.1 the task execution times measured in the three tests at the points investigated are compared to the computed TPI values. The highest TPI values and the shortes execution times (i.e. the best expected and measured performances) are highlighted by bold and underlined font. The execution times collected in Table 4.1 refer to five complete pick-and-place tasks (comprising five movements from sp to ep and five movements ep to sp) carried out about all the investigated points. They have been computed by averaging the times recorded in four independent repetitions of the same set of five pick-and-place tasks.

It can be noticed that the TPI values provide predictions coherent with the measured times: in general, the higher the TPI values the shorter the execution times. Moreover, in all the tests, rises and falls of the execution times are in excellent agreement with the opposite trends of TPI values.

Table 4.1 Measured execution times vs. TPI values

	Test 1			**Test 2**			**Test 3**		
k	$(z_{rp})_k$ [mm]	Task execution time [s]	TPI	$(x_{rp})_k$ [mm]	Task execution time [s]	TPI	$(z_{rp})_k$ [mm]	Task execution time [s]	TPI
1	-780	4.876	0.7095	500	-	-	-780	4.876	0.7101
2	-800	4.792	0.7447	450	-	-	-800	4.852	0.7455
3	-820	4.792	0.7785	400	-	-	-820	4.792	0.7794
4	-840	4.748	0.8111	350	4.740	0.8276	-840	4.785	0.8121
5	-860	4.708	0.8424	300	4.740	0.8577	-860	4.708	0.8435
6	-880	4.708	0.8726	250	4.740	0.8830	-880	4.708	0.8738
7	-900	4.708	0.9017	200	4.716	0.9033	-900	4.708	0.9030
8	-920	4.668	0.9297	150	4.700	0.9185	-920	4.674	0.9312
9	-940	4.668	**0.9320**	100	**4.620**	0.9285	-940	**4.664**	**0.9320**
10	-960	**4.664**	0.9108	50	**4.620**	**0.9332**	-960	4.674	0.9092
11	-980	**4.664**	0.8896	0	**4.620**	0.9326	-980	4.668	0.8880
12	-1000	4.668	0.8700	-50	**4.620**	0.9267	-1000	4.668	0.8683
13	-1020	4.688	0.8517	-100	4.688	0.9154	-1020	4.697	0.8500
14	-1040	4.688	0.8347	-150	4.712	0.8990	-1040	4.708	0.8329
15	-1060	4.708	0.8189	-200	4.752	0.8776	-1060	4.708	0.8170
16	-1080	4.708	0.8042	-250	4.748	0.8512	-1080	4.748	0.8023
17	-1100	4.750	0.7906	-300	4.760	0.8199	-1100	4.752	0.7886
18	-1120	4.762	0.7782	-350	4.784	0.7833	-1120	4.752	0.7761
19	-1140	4.772	0.7669	-400	-	-	-1140	4.792	0.7647
20	-1160	4.796	0.7569	-450	-	-	-1160	4.852	0.7545
21	-1180	4.836	0.7483	-500	-	-	-1180	4.952	0.7456

The TPI based seek for the optimal robot/task position would lead to the selection of rp_9 in Test 1 and 3, and of rp_{10} in Test 2. In Test 2 and 3 the same choice would be made by considering the experimental execution times. In Test 1 the slight

discrepancy between the best expected and measured performances would lead to the selection of an adjacent point just 20 mm below the computed optimum (rp_{10}).

Table 4.2 Time differences and time reductions

	Test 1	**Test 2**	**Test 3**
T_{max}-T_{min}	0.212 s	0.164 s	0.288 s
Performance improvement	4.45%	3.55%	6.17%

Finally, Table 4.2 highlights the differences between the maximum (T_{max}) and the minimum (T_{min}) execution times recorded in each test and the performance improvement that can therefore be achieved by just varying the task position within the workspace. Such a performance improvement can be appreciated better by translating it in terms of increase in picks-per-minute (ppm): a key performance indicator for industrial 4-RUU parallel robots. For example, by referring to the results obtained in Test 3 if the robot could operate at 120 ppm in the worst performance region, productivity could be boosted to a level of 127 ppm in the region with maximum TPI. If the robot operates three shifts per day it means that as much as ten thousand further picks per day can be performed, by just selecting the best robot/task relative position predicted through the TPI.

5 GEOMETRIC OPTIMIZATION OF PARALLEL ROBOT LINK LENGTHS BASED ON TPI MAXIMIZATION

5.1. Optimization methodologies for robots design

Parallel robots have remarkable advantages for many applications over the serial ones in terms of rigidity, accurate positioning, high velocities.

The performances of such robots are very sensitive to the mechanism dimensions. Consequently, the geometrical synthesis of the mechanisms cannot be dissociated from the analysis of performance indexes or criterions for characterizing the behavior of manipulators. Several optimization methodologies have been proposed for design purposes. Such methods usually concern robot topology (e.g. joint layout) or the sizing of a given robot (e.g. link lengths).

Some approaches have been presented in Chapter 4. They focus on the optimization of the design configuration of a given manipulator ([GOSSELIN 1989], [MAYORGA 1997], [KHATAMI 2002], [MAYORGA 2005], [FATTAH 2002]) and on the optimization of robot architecture by considering several criteria simultaneously ([STOUGHTON 1993], [STOCK 2003], [LI 2004]).

There are other optimization methodologies worthy of mention. Among these, the atlases of GCI used in [GAO 1995B] and [GAO 1998] for optimizing the link lengths of 2-DOF planar parallel manipulators. Another one has been analyzed in [GAO 1995]. In such a paper the solution space of manipulators has been used to study various performances of robotic mechanisms and to select optimum manipulators.

In 2000, Carretero et al. proposed the architecture optimization allowing minimization of parasitic motion, i.e., motions in the three unspecified motion coordinates [CARRETERO 2000]. In the same year Liu et al. applied the concepts of dexterity and stiffness for optimizing the link lengths of manipulators and analyzing the behavior of 3-DOF spatial parallel manipulators on the reachable workspace [LIU 2000].

Subsequently, in [OTTAVIANO 2001] a formulation for optimum design of a 3-DOF spatial parallel manipulator was developed in order to obtain designed parameters of a robot whose position workspace is suitably prescribed. In [RYU 2001] by minimizing the error amplification and considering the workspace, architecture singularity, and design variable limits a design optimization of the HexaSlide type parallel manipulator had been performed. Some years later, the architecture optimization of a 3-DOF translational parallel mechanism has been carried out on the basis of a prescribed Cartesian workspace with prescribed kinetostatic performances in [CHABLAT 2003]. A method to maximize the stiffness has been suggested in [KIM 2003] in order to minimize the deflection at the joints caused by the bending moment. Successively, the optimal dimensional synthesis of the 2-DOF translational parallel robot was achieved in [HUANG 2004] by minimizing a global and comprehensive conditioning index subject to a set of appropriate constraints. A different approach for the optimization of the kinematic optimization of parallel robots has been proposed in [MILLER 2004]. In this work Miller combined two performance indices in order to obtain architectures which yield an optimum compromise between manipulability and the space utilization index. In [LOU 2005] an optimization algorithm has been

proposed to maximize the regular workspace of parallel robots. In recent years genetic algorithms and artificial neural networks intelligent have been implemented for the dimensional synthesis of the spatial six degree-of-freedom (DOF) parallel manipulator [GAO 2010]. Moreover Zhao et al. exploited the least number method for variables in order to optimize the leg length of a spatial parallel manipulator for the purpose of obtaining a dexterous workspace [ZHAO 2007].

In [TSAI 2010] the global condition index has been applied for optimizing architecture of the 3-UPU manipulator.

In literature there has not been a unified method for the robot design and it can be of primary importance to study some useful methods which allow to understand the relationships between the criteria and link lengths of the manipulators.

Therefore, this Chapter addresses the problem of the sizing of a given robot (e.g. link lengths) by translating the optimization problem into the problem of choosing the lengths of some selected robot links maximizing a suitably defined performance index.

5.2. Formulation of Geometric Optimization Problem

The proposed optimization methodology is based on the TPI maximization accounting for the task that has to be carried out by the robot. Some of the most important features of such an index are briefly described here (refer to Chapter 3 for a complete description). Basically, the TPI is defined as a weighted average of the DSI values related to each *i*-th elementary displacement (i.e. straight-line

segment) of length l_i into which the path of the task can be split. The weights are computed by comparing the length of the *i*-th segment to the total length of the task path. Such an average leads to the following straightforward TPI definition:

$$\mathrm{TPI} = \frac{\sum_{i=1}^{n} \mu_{Ri} \cdot l_i}{\sum_{i=1}^{n} l_i} \tag{5.1}$$

where *n* is the number of straight-line segments into which the path is split. This analytical expression is invariant with respect to the choice of the fixed reference frame.

The optimization approach is based on the search of the lengths of the robot links which maximize the TPI. The corresponding objective function is:

$$\max\ (\mathrm{TPI}) \tag{5.2}$$

Whereas, when the task is composed by a sequence of subtasks about different positions, the objective function becomes:

$$\max\ (\mathrm{TPI_A}) \tag{5.3}$$

where $\mathrm{TPI_A}$ is the average of the TPIs related to each subtask and referred to the subtask reference points.

Moreover, in the optimal geometric design of parallel manipulators a set of appropriate constraints should be considered in order to ensure that the resulting structure is practical. Such constraints could regard for example the workspace, the range of the links lengths or the actuators. Hence the range of the design parameters should be established according to the corresponding limits.

The proposed method can therefore be applied to any parallel robot architectures, as long as an inverse Jacobian matrix can be computed and parameters constraints can be expressed.

5.3. Numerical Examples and Discussion

The optimization methodology is illustrated with examples involving the four-leg delta-like Adept Quattro parallel manipulator, which has been already presented in Chapter 2. Table 5.1 collects the chief geometrical parameters of the Quattro robot and of its workspace (refer to Fig.5.1 for the meaning of each parameter).

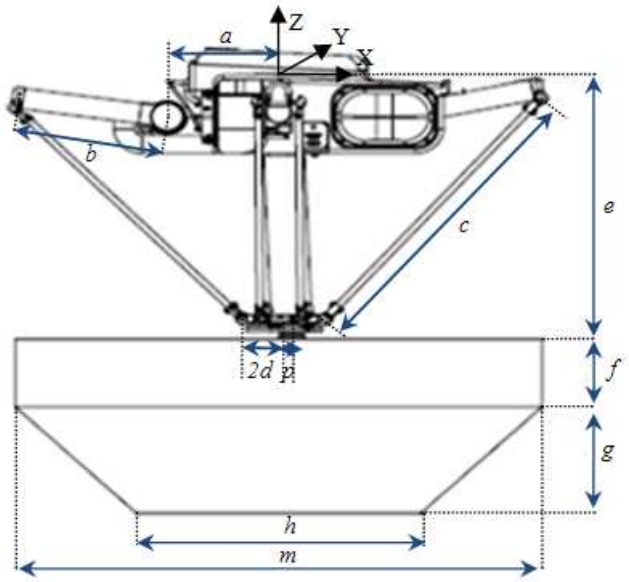

Fig. 5.1 Schematic representation of the Adept Quattro^{TM} and of its workspace.

Table 5.1 Geometrical parameters of the Quattro robot and of its workspace.

Symbol	***Values [mm]***
a	275
b	375
c	825
d	75
e	780
f	220
g	200
h	700
m	1140
p	30.8

The identical lengths *c* of the Quattro eight connecting rods (four twin rods) have been optimized with respect to tasks based on repetitions of the conventional "pick-and-place" movement.

The choice of optimizing the length *c* of the connecting rods is a consequence of the practical evidence that in most delta-like industrial robots connecting rods are the links that can be most promptly replaced if necessary (see ABB IRB 340 manipulator or IRB 360). Indeed, the procedure for attaching and detaching the twin rods of the Quattro robot to the platform and to the crank arms is very fast and simple.

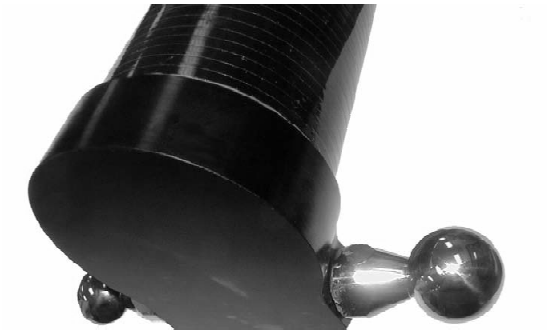

Fig. 5.2 Crank arm ball studs.

Let us consider, for instance, the attaching of the connecting rods to a crank (refer to Figs. 5.2 and 5.3). Such rods are previously assembled in pairs with two springs at each end. Moreover the rods have a ball joint socket at each end, whereas the crank arms have mating pairs of ball studs.

Fig. 5.4 Installing ball joints.

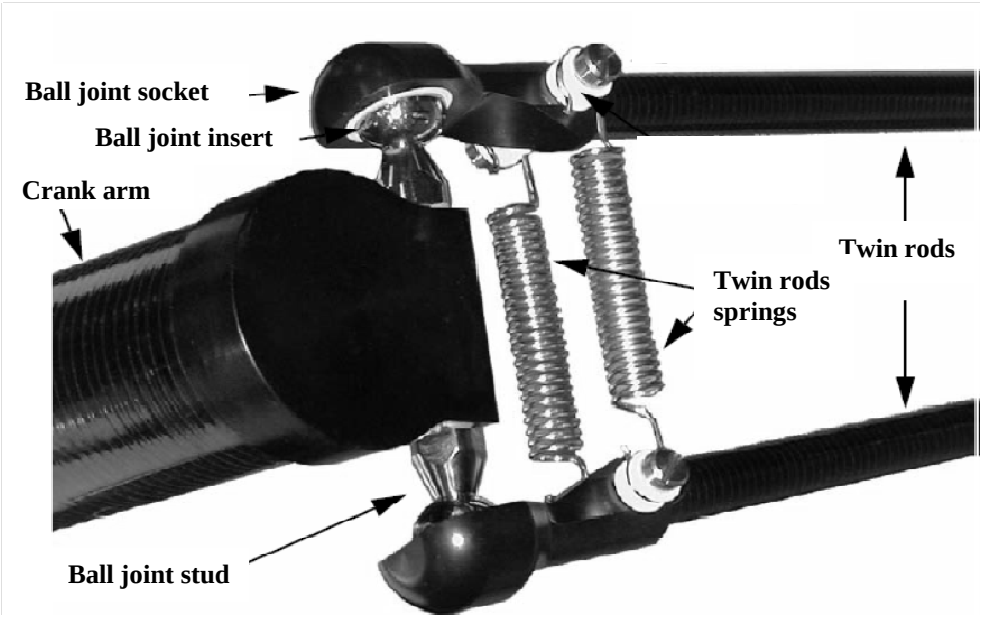

Fig. 5.3 Twin rods and crank arm completely assembled.

Each ball joint socket has to be slipped over the corresponding ball, as can be appreciated in Fig. 5.4.

The same procedure has to be repeated for connecting a pair of rods to one of the four pairs of ball studs on the platform. It must be noted that no tools are needed for the abovementioned operations.

In the optimal geometric design of the parallel manipulator under consideration, a set of appropriate constraints have been taken into account.

The first one is related to the design variable *c*. Such a parameter is characterized by discrete variations, according to prescribed steps (5 mm), and is constrained so that: $c_{min} \leq c \leq c_{max}$, (with c_{min}= 550 mm and c_{max} = 950 mm) in order to ensure technically feasible solutions.

Typically, a parallel robot is designed to be mounted above a work area suspended on a frame. Such a mounting frame is usually constructed of welded steel members so that the structure can be adequately stiff to hold the robot rigidly in place while the robot platform moves around the workspace. Obviously, once the frame has been manufactured and positioned in a production line and the robot has been mounted, the frame cannot be changed.

For this practical reason, some physical space constrains have been considered in the maximization problem. In fact, the TPI or TPI_A values are studied within the Quattro workspace characterized by the nominal workspace parameters (see *e*, *f*, *g*, *h*, *m* parameters in Table 5.1).

In addition to the just mentioned constraints, other practical constraints regarding the actuators limitations can be included in the optimization problem.

For every end-effector pose $(x_0, y_0, z_0, \theta_0)$, using the inverse kinematics, the active joint coordinates φ_i can be mathematically expressed as follows:

$$\varphi_{min} \leq \varphi_i(x_0, y_0, z_0, \theta_0) \leq \varphi_{max} \tag{5.3}$$

where i = 1, 2, 3, 4 and φ_{min} and φ_{max} are respectively lower bound and upper bound for *i*-th actuator due to actuator limits and/or mechanical interference between links.

The lower and upper joint angle limits are set at φ_{min}= -150° and φ_{max}= 75°. Referring to the Fig. 5.5 the angle φ assume positive values when the coordinate of the Universal joint (U) is positive, i.e. $z_U > 0$, and negative when $z_U < 0$.

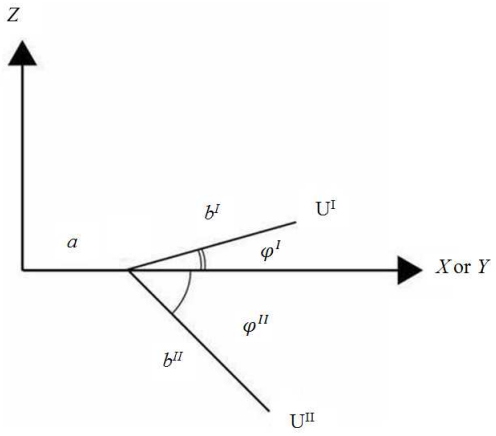

Fig. 5.5 Schematic representation of the angle φ: $\varphi^I > 0$ and $\varphi^{II} < 0$.

The standard pick-and-place task considered comprises two identical short vertical straight line translations and a longer horizontal one (in detail, L_{v1}= L_{v2}=25mm, L_h=305mm, l_i=5mm).

In order to locate the pick-and-place path in the workspace and hence to check whether or not it can be entirely executed keeping the end effector within the workspace, a reference point rp has been defined. Such a point can be chosen arbitrarily (either belonging to the path or not). However, in case of symmetrical paths, the path midpoint of the sequence of movements is an intuitive and simple choice, which has been adopted in this work.

Two sample optimization test cases have been analyzed and are discussed. They differ in the features of the task to be carried out:

- Test 1: a single pick-and-place task ;
- Test 2: a task composed by a sequence of two pick-and-place subtasks about two different positions.

Six independent tests for optimizing the robot geometry have been computed and discussed. Three with the L_h segment parallel to the *X* axis of the world reference frame (Test 1A, Test 2A and Test 2B), the others with the L_h segment parallel to the *Y* axis (Test 1B, Test 2C and Test 2D). In all the tests the performance index values have been evaluated in one path reference point (Test 1) or two path reference points (Test 2). The Cartesian coordinates of the path reference points (in millimeters, and referred to the robot world reference frame) and the results of the test cases analyzed are shown in Table 5.2 for Test 1 and in Table 5.3 for Test 2.

Table 5.2 Locations of the reference points and results of Test 1.

Test 1	**A**	**B**
rp_1	(-300, 200, -780)	(-50, -100, -1000)
Optimized value of *c* [mm]	**740**	**950**

Table 5.3 Locations of the reference points and results of Test 2.

Test 2	**A**	**B**	**C**	**D**
rp_1	(0, 50, -790)	(400, 0, -800)	(400, 200, -830)	(400, 350, -850)
rp_2	(-50, 10, -900)	(100, 30, -950)	(400, 200, -920)	(-100, -300, -980)
Optimized value of *c* [mm]	**610**	**760**	**820**	**885**

Figures 5.6, 5.8, 5.10, 5.12, 5.14, 5.16 show a basic kinematic scheme of the robot (in blue before optimization, in pink after optimization) and the paths of the task analyzed. All the tasks considered in the tests can be executed, since all their points belong to the robot workspace. Consequently, all tests do not possess unfeasible reference points. In Fig 5.6 the reduction of the length of *c* after optimization with respect to the nominal one can be observed. The difference between the two lengths is equal to 95 mm. In Figs.5.7, 5.9 the variation of the TPI values computed at rp_1 are related to admissible length *c*. In Figs 5.11, 5.13, 5.15, 5.17 the $TPIs_A$ (the mean between the values computed at rp_1 and rp_2) are related to admissible length *c*. The optimal values for each test can be easily inferred from the plots and it can be noticed the evolution of the index by varying the connecting rods length. Clearly, the optimal length is in correspondence of the maximum value of the index.

This study seeks a good formulation for optimal design of a four-leg delta-like parallel robot, but it can be applied to any parallel robot architectures.

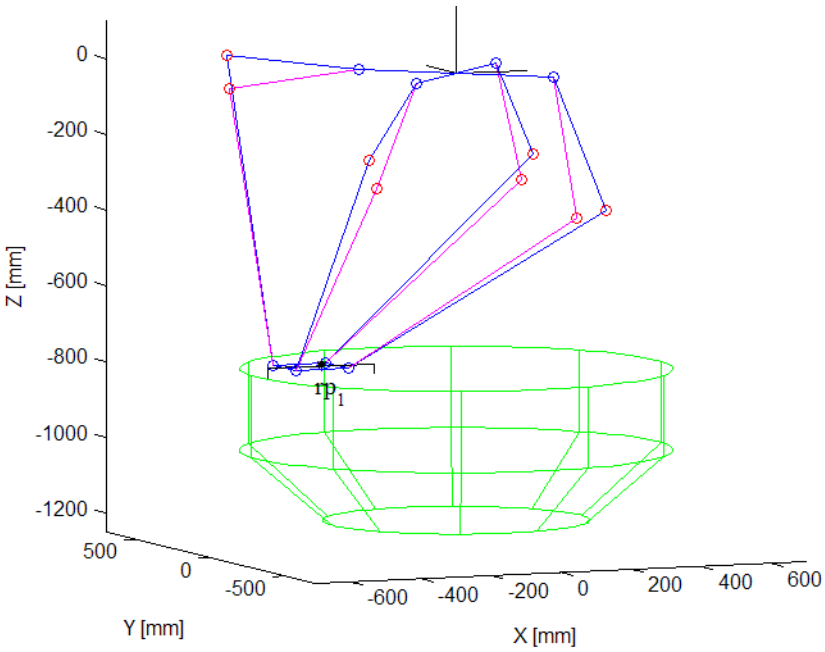

Fig. 5.6 Spatial view of one task path of Test 1A before optimization (in blue) and after optimization (in pink).

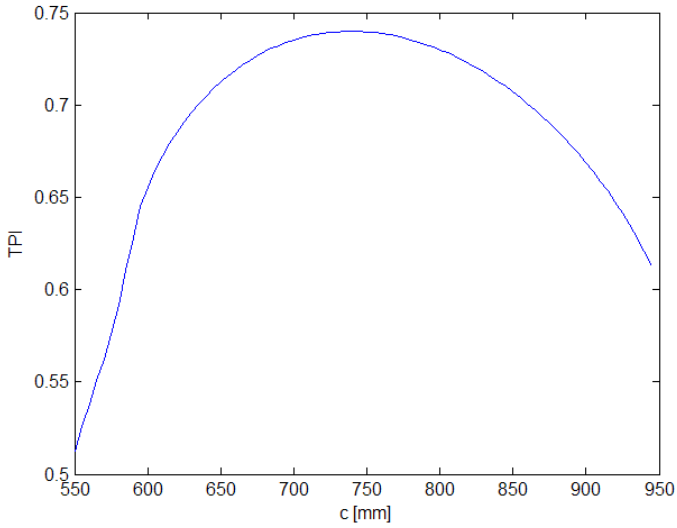

Fig. 5.7 Connecting rod length (*c*) vs. TPI of Test 1A.

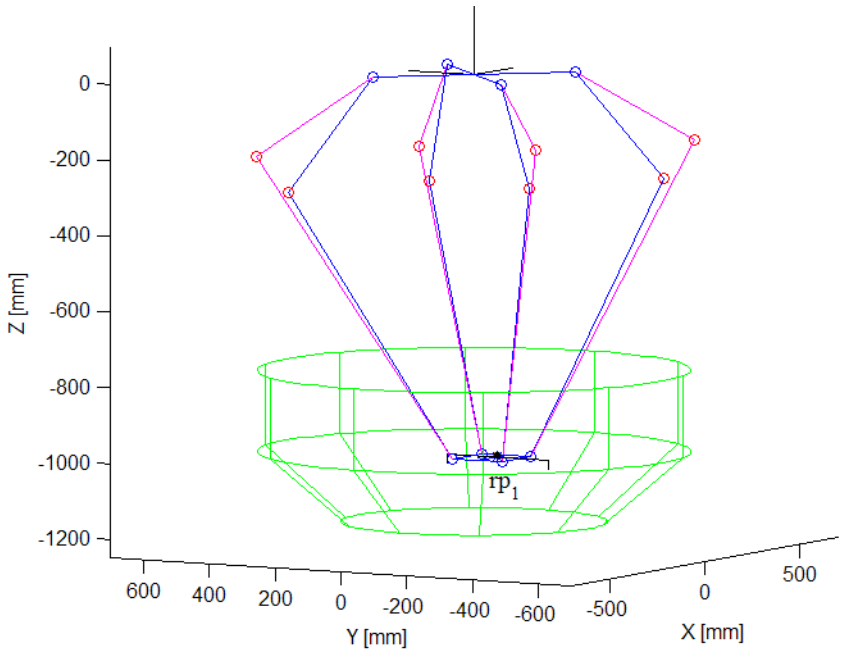

Fig. 5.8 Spatial view of one task path of Test 1B before optimization (in blue) and after optimization (in pink).

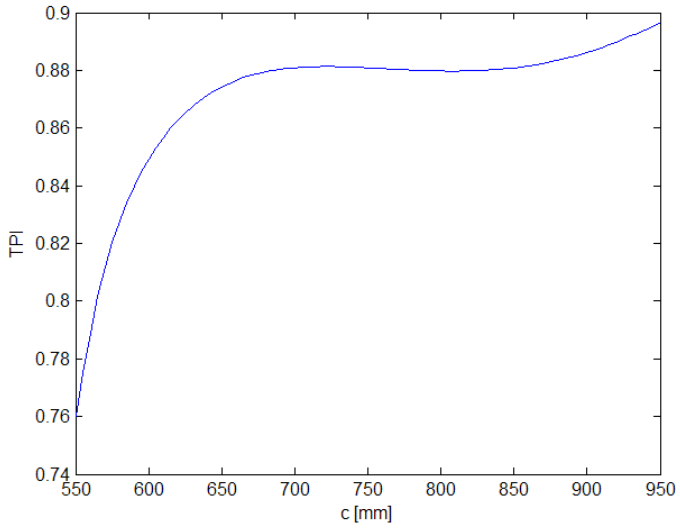

Fig. 5.9 Connecting rod length (*c*) vs. TPI of Test 1B.

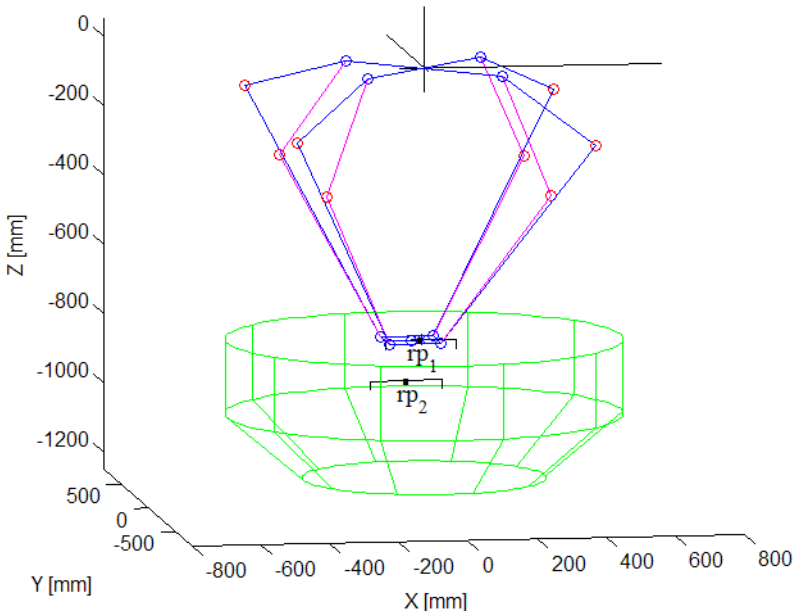

Fig. 5.10 Spatial view of two subtasks of Test 2A and of the manipulator before optimization (in blue) and after optimization (in pink).

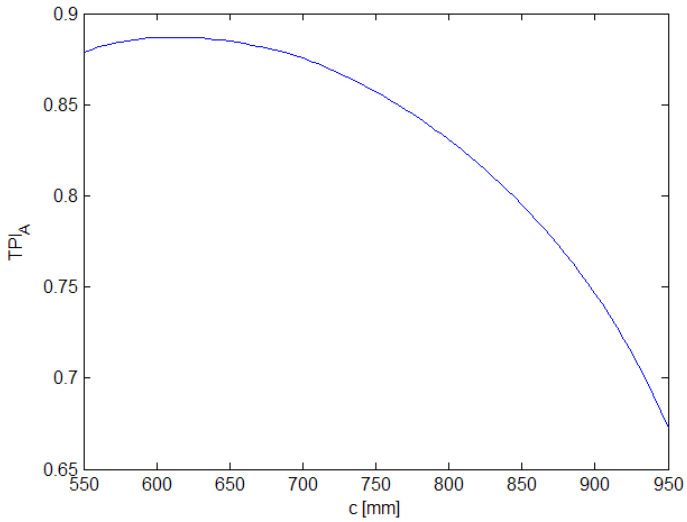

Fig. 5.11 Connecting rod length (c) vs. TPI_A of Test 2A.

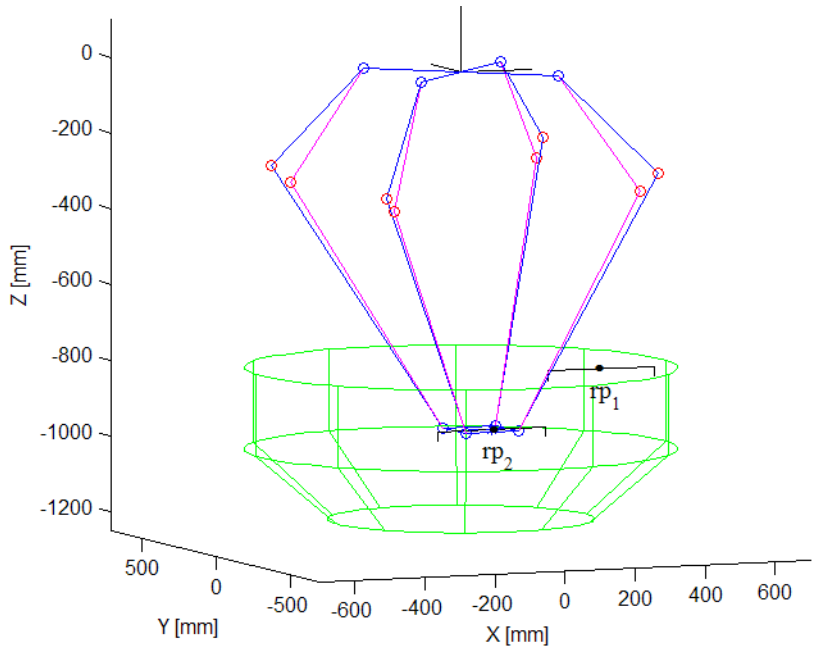

Fig. 5.12 Spatial view of two subtasks of Test 2B and of the manipulator before optimization (in blue) and after optimization (in pink).

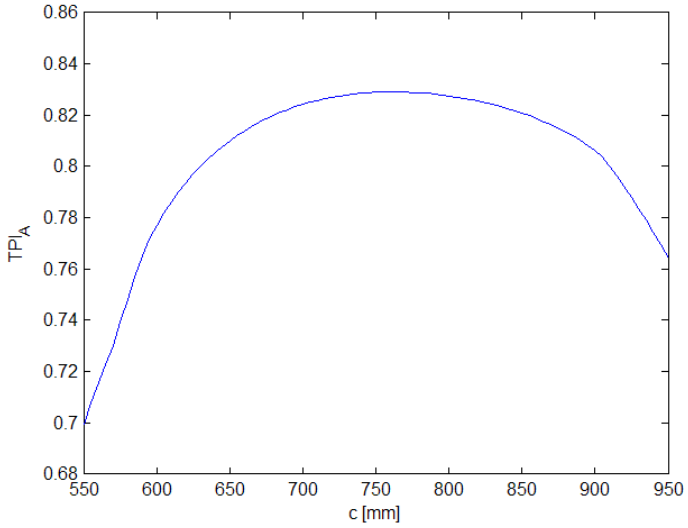

Fig. 5.13 Connecting rod length (c) vs. TPI_A of Test 2B.

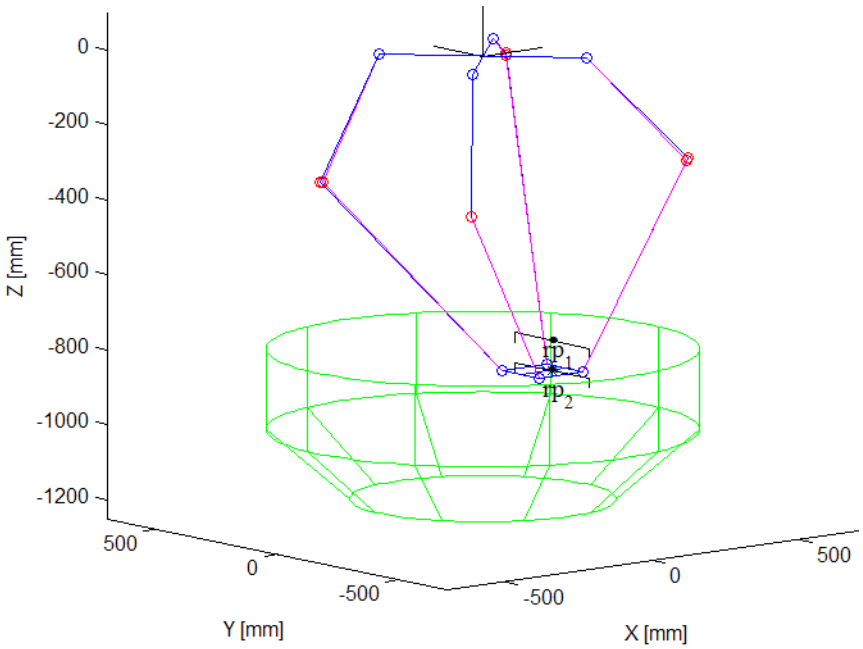

Fig. 5.14 Spatial view of two subtasks of Test 2C and of the manipulator before optimization (in blue) and after optimization (in pink).

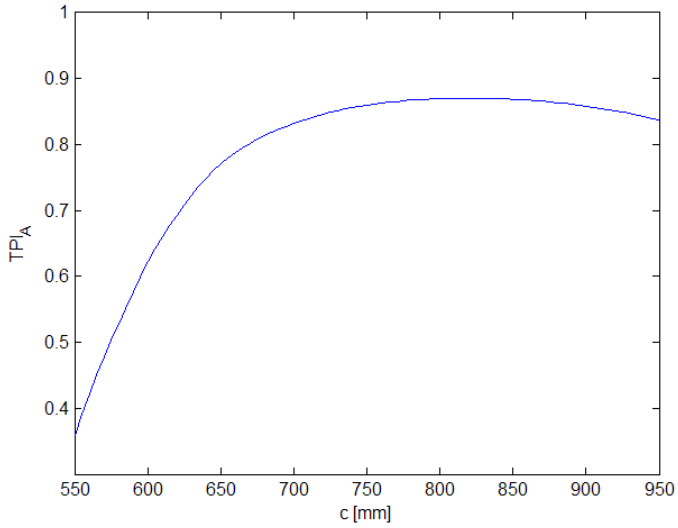

Fig. 5.15 Connecting rod length (c) vs. TPI_A of Test 2C.

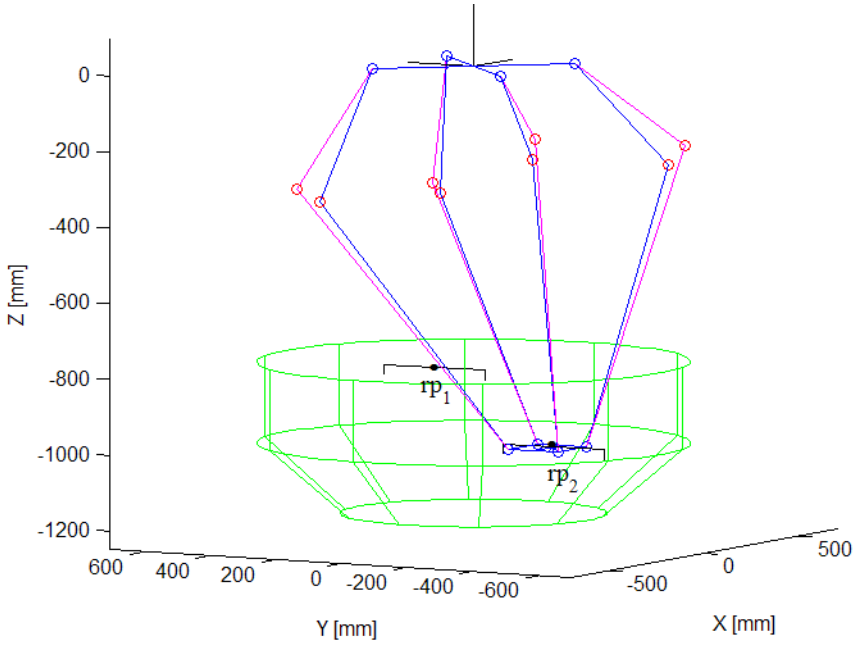

Fig. 5.16 Spatial view of two subtasks of Test 2D and of the manipulator before optimization (in blue) and after optimization (in pink).

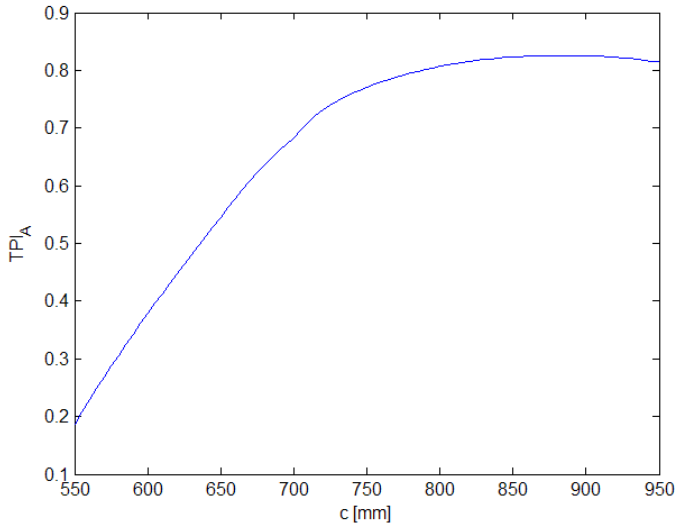

Fig. 5.17 Connecting rod length (c) vs. TPI_A of Test 2D.

CONCLUSIONS

In this Thesis novel performance indexes for parallel manipulators are presented.

The experimental investigation carried out on a suitably instrumented Adept Quattro commercial robot has proved that the proposed Direction Selective Indexes (DSIs) formulation can provide reliable predictions of the robot performances in making movements along specific directions. Overall the predictions made through the DSIs are considerably more accurate than the predictions provided by manipulability indexes.

So far, the effectiveness of DSIs has been assessed on a single family of parallel manipulators (4- RUU) but the results achieved are thought to have a general relevance: DSI definition just recourse to vectors extracted by the inverse Jacobian matrix and includes no constraints accounting for a specific parallel robot architecture. The proposed indexes can therefore be applied to any parallel robot architecture, as long as an inverse Jacobian matrix can be computed. DSIs, though being purely kinematic indexes, may provide useful hints in foreseeing the robot dynamic performances along relevant directions of motion within the workspace. At robot design, installation or programming stages, such information could be usefully employed to optimize the robot geometrical features, the robot location within a workcell, the location of the target frames with respect to the robot, and also the robot end-effector paths. All these considerations make the DSIs a useful tool for robot designers, manufacturers and programmers.

Afterwards, a new Task dependent Performance Index (TPI) has been defined based on the extended DSI formulation. TPI is an index aimed at providing evaluations of parallel robot performances in executing specific tasks. What is innovative in the TPI, is its accounting for robot kinematics and task geometrical features concurrently. This is a consequence of both using DSI in the TPI formulation and explicitly considering the length and direction of the sequence of translations into which the task path can be split.

Hence, TPI is an index which can be successfully employed in optimal robot positioning: by seeking for the task position within the workspace providing the maximum TPI value it is possible to infer the best relative position between a robot and a task. Such a result can be exploited to either optimally locate the task within the robot workspace, or, if the task location cannot be modified, to identify the best robot base location within a workcell.

The experimental investigations carried out on a commercial parallel robot have proved that the proposed TPI formulation can provide reliable predictions of the best relative positioning between the robot and the task to be executed. In particular, TPI validation has been carried out through independent experiments, by supposing to have to accomplish different pick-and-place tasks based on a typical benchmark motion pattern. The execution times recorded to carry out the selected tasks at different locations within the workspace have been compared with the TPI values computed at the same locations. In all the experiments, such a comparison has highlighted a very good correspondence between the best relative positioning inferable by seeking for the maximum TPI value and the actual behavior of the robot.

Not only do the results achieved show the effectiveness of the method and its capability to provide unique and global optimal solutions, but they also highlight its wide applicability to different mechanical design tasks. Clearly the versatility of the proposed approach.

The results achieved are believed to have a general validity which goes beyond the test cases and the manipulator proposed here, which are to be considered as mere examples.

The TPI has also been employed as a design tool in an optimization methodology for choosing the lengths of some selected robot links. The results discussed refer to a single parallel robot family and to specific tasks but they are believed to prove the effectiveness of the method and its generality of applicability.

List of publications

The major outcomes of this research may be found in the following references:

- G.Boschetti, R.Rosa, A.Trevisani, “Parallel Robot Translational Performance Evaluation through Direction Selective Index (DSI),” Journal of Robotics 2011, Article ID 129506, 14 pages.

- G.Boschetti, R.Caracciolo, R.Rosa, A.Trevisani, “Manipulability vs. Direction Selective Indexes: a Numerical and Experimental Investigation,” In Proceedings of the 4th International Congress Design and Modeling of Mechanical Systems:CMSM’2011.
- G.Boschetti, R.Caracciolo, R.Rosa, A.Trevisani, “Generalizing the Formulation of the Direction Selective Index for Parallel Robot Performance Assessment along a Generic Direction,” submitted to the ASME 2012 11th Biennial Conference On Engineering Systems Design And Analysis (ESDA2012) in December 2011 for possible publication.
- G. Boschetti, R. Caracciolo, R. Rosa, A. Trevisani, “Geometric optimization of parallel robot link lengths based on performance index maximization,” submitted to the ASME 2012 11th Biennial Conference On Engineering Systems Design And Analysis (ESDA2012) in December 2011 for possible publication.

References

[ANGELES 1992] J.Angeles and C.S.Lopez-Cajun, “Kinematic Isotropy and the Conditioning Index of Serial Robotic Manipulators,” The International Journal of Robotic Research 11, 6 (1992) 560-571.

[BOSCHETTI 2010] G.Boschetti and A.Trevisani, “Direction Selective Performance Indexes for Parallel Manipulators,” Proceedings of the 1st Joint International Conference on Multibody System Dynamics, Lappeenranta, Finland, May 25-27, 2010.

[CHEDMAIL 1996] P.Chedmail, E.Ramstein, “Robot Mechanism Synthesis and Genetic Algorithm,” Proceedings of IEEE, International Conference on Robotics and Automation (1996) 4.

[COMPANY 2009] O.Company, F.Pierrot, S.Krut and V.Nabat, “Simplified dynamic modeling and improvement of a four-degree-of-freedom pick-and-place manipulator with articulated moving platform,” Proceedings of IMechE Part I: Journal of Systems and Control Engineering 223, 1 (2009) 13-2.

[FATTAH 2002] A.Fattah, A.M. Hasan Ghasemi, “Isotropic Design of Spatial Parallel Manipulators,” International Journal of Robotics Research (2002) 21:811-82.

[GAO 1995A] Feng Gao, X.Q. Zhang, W.B. Zu, Y.S. Zhao, Distribution of some properties in a physical model os the solution space of 2-DOF parallel planar manipulators, Mechanism and Machine Theory 30 (6) (1995) 811-817.

[GAO 1995B] Feng Gao, Xin-jun Liu, W.A. Gruver, The global conditioning index in the solution space of two Degree-of- Freedom planar parallel manipulators, in: IEEE SMC'95,Canada, (1995) 4055-4058.

[GAO 1998] Feng Gao, Xin-Jun Liu, W.A. Gruver, Performance evaluation of two degrees-of-freedom planar parallel robots, Mechanism and Machine Theory 33 (2) (1998) 661-668.

[GOSSELIN 1989] C.Gosselin, J.Angeles, "The optimum kinematic design of a spherical three-degee-of-freedom parallel manipulator," Journal of Mechanisms, Transmissions and Automation in Design (1989) 111.

[GOSSELLIN 1990] C.Gosselin, "Stiffness mapping for parallel manipulators," IEEE Transaction on Robotics and Automation 6, 3 (1990) 377–82.

[GOSSELIN 1991] C.Gosselin and J.Angeles, "A global performance index for the kinematic optimization of robotic manipulators," Transaction of the ASME, Journal of Mechanical Design 113 (1991) 220-226.

[GOSSELIN 1992] C.M. Gosselin, "The optimum design of robotic manipulators using dexterity indices," Journal of Robotics and Autonomous System 9, 4 (1992) 213-226.

[KHATAMI 2002] S.Khatami, F.Sassani, "Isotropic Design Optimization of Robotic Manipulators Using a Genetic Algorithm Method," In: Proceedings of IEEE, Intl. Symposium on Intelligent Control Oct 27 30, 2002.

[KLEIN 1987] C.Klein and B.Blaho, " Dexterity measures for the design and control of kinematically redundant manipulators," The International Journal of Robotics Research 6(2), (1987) 72-83.

[KIM 2003] S.G.Kim and J.Ryu, “New Dimensionally Homogeneous Jacobian Matrix Formulation by Three End-Effector Points for Optimal Design of Parallel Manipulator,” IEEE Transactions on Robotics and Automation 19, 4 (2003) 731-737.

[KIM 2004] S.G.Kim and J.Ryu, “Force Transmission Analyses with Dimensional Homogeneous Jacobian Matrices for Parallel Manipulators,” KSME International Journal 18, 5 (2004) 780-788.

[LI 2004] Y.Li, Q.Xu, “Optimal kinematic design for a general 3-PRS spatial parallel manipulator based on dexterity and workspace,” Proceedings of the Eleventh International Conference on Machine Design and Production, Antalya, Turkey, October 13-15, 2004.

[LI 2006A] Y.Li and Q.Xu, “A New Approach to the Architecture Optimization of a General 3-PUU Translational Parallel Manipulator,” Journal of Intelligent and Robotic Systems 46, 1 (2006) 59-72.

[LI 2006B] Y.Li and Q.Xu, “Kinematic Analysis and Design of a New 3-DOF Translational Parallel Manipulator,” Journal of Mechanical Design, Transactions of the ASME 128, 4 (2006) 729 737.

[MA 1991] O.Ma and J.Angeles, “Optimum Architecture Design of Platform Manipulator,” Proceedings of the IEEE International Conference on Robotics Automation (1991) 1131-1135.

[MANSOURI 2009] I.Mansouri and M.Ouali, “A new homogeneous manipulability measure of robot manipulators, based on power concept,” Mechatronics 19 (2009) 927-944.

[MANSOURI 2011] I.Mansouri and M.Ouali, “The power manipulability–A new homogeneous performance index of robot manipulators,” Robotics and Computer-Integrated Manufactoring 27 (2011) 434-449.

[MAYORGA 1997] R.V.Mayorga, E.D.de Leon Optimal, “Upper Bound Conditioning for Manipulator Kinematic Design Optimization,” IEEE, (1997).

[MAYORGA 2005] R.V.Mayorga, J.Carrera, M.M.Oritz, “A kinematics performance index based on the rate of change of a standard isotropy condition for robot design optimization,” Robotics and Autonomous Systems (2005) 53:153-163.

[MAYORGA 2006] R.V.Mayorga and J.Carrera, “A manipulator performance index based on the jacobian rate of change: a motion planning analysis,” Proceedings of the 2006 IEEE International Conference on Robotics and Automation, Orlando, Florida, May 2006.

[MERLET 2006] J.P.Merlet, “Jacobian, manipulability, condition number, and accuracy of parallel robots,” Transaction of the ASME, Journal of Mechanical Design 128 (2006) 199-206.

[MITSI 2008] S.Mitsi, K.D.Bouzakis, D.Sagris, G.Mansour, “Determination of optimum robot base location considering discrete end-effector position by means of hybrid genetic algorithm,” Robotics and Computer-Integrated Manufacturing (2008) 24:50–9.

[PETIOT 1998] J.Petiot, P.Chedmail, J.Y.Haschoet, “Contribution to the scheduling of trajectories in robotics,” Robotics and Computer-Integrated Manufacturing journal (1998) 14:237-51.

[POND 2006] G.Pond and J.A.Carretero, “Formulating Jacobian matrices for the dexterity analysis of parallel manipulators,” Mechanism and Machine Theory 41 (2006) 1505-1519.

[SALISBURY 1982A] J.K.Salisbury and J.J. Craig “Articulated hands: force control and kinematic issues,” The International Journal of Robotics Research 1, (1982) 4-17.

[SALISBURY 1982B] J.Angeles and C.S.Lopez-Cajun, “The dexterity index of serial-type robotic manipulators”, ASME Trends and Developments in Mechanisms, Machines and Robotics (1988) 79–84.

[STAN 2008] S.Stan, V.Mătieş, Bălan, “Kinematic analysis, design and optimization of a six degrees-of-freedom parallel robot” Proceedings of ENOC 2008, Saint Petersburg, Russia, June, 30-July, 2008; 4.

[STOCK 2003] M.Stock, K.Miller, “Optimal Kinematic Design of Spatial Parallel Manipulators,” Application to Linear Delta Robot. ASME Journal of Mechanical Design (2003) 125(2): 292-301.

[STOUGHTON 1993] R.S.Stoughton, T.Arai, “A Modified Stewart Platform Manipulator with Improved Dexterity,” IEEE Transactions on Robotics and Automation (1993) 9(2): 166-173.

[TSAI 2010] L. W .Tsai, “Kinematics and optimization of a spatial 3-upu parallel manipulator,” ASME Journal of Mechanical Design (2000) 122:439–446.

[WANG 2010] J.Wang, C.Wu and X.J.Liu, “Performance evaluation of parallel manipulators: Motion/force transmissibility and its index,” Mechanism and Machine Theory 45 (2010) 1462–1476.

[XU 2008] Q.Xu and Y.Li, “An Investigation on Mobility and Stiffness of a 3-DOF Translational Parallel Manipulator via Screw Theory,” Robotics and Computer-Integrated Manufacturing 24, 3 (2008) 402-414.

[YOSHIKAWA 1985] T.Yoshikawa, “Manipulability of Robotic Mechanisms,” The International Journal of Robotics Research 4, (1985) 3-9.

[ZACHARIA 2005] P.T.Zacharia, N.A.Aspragathos, “Optimal Robot Task Scheduling based on Genetic Algorithms,” Robotics and Computer-Integrated Manufacturing journal (2005) 21(1) 67-79.

[ZHAO 2007] J.S.Zhao, S.L.Zhang, J.X.Dong, Z.J.Feng, K.Zhou, “Optimizing the kinematic chains for a spatial parallel manipulator via searching the desired dexterous workspace,”Robotics and Compututer Integrated Manufacturing (2007) 23(1) 38–46.